Available online at www.sciencedirect.com
ScienceDirect
Computer Coupling of Phase Diagrams and Thermochemistry 32 (2008) 268–294
www.elsevier.com/locate/calphad

An introduction to phase-field modeling of microstructure evolution

Nele Moelans*, Bart Blanpain, Patrick Wollants

Department of Metallurgy and Materials Engineering, Faculty of Engineering, Katholieke Universiteit Leuven, Kasteelpark Arenberg 44, B-3001 Leuven, Belgium

Received 1 June 2007; received in revised form 10 October 2007; accepted 1 November 2007
Available online 21 December 2007

Abstract

The phase-field method has become an important and extremely versatile technique for simulating microstructure evolution at the mesoscale. Thanks to the diffuse-interface approach, it allows us to study the evolution of arbitrary complex grain morphologies without any presumption on their shape or mutual distribution. It is also straightforward to account for different thermodynamic driving forces for microstructure evolution, such as bulk and interfacial energy, elastic energy and electric or magnetic energy, and the effect of different transport processes, such as mass diffusion, heat conduction and convection. The purpose of the paper is to give an introduction to the phase-field modeling technique. The concept of diffuse interfaces, the phase-field variables, the thermodynamic driving force for microstructure evolution and the kinetic phase-field equations are introduced. Furthermore, common techniques for parameter determination and numerical solution of the equations are discussed. To show the variety in phase-field models, different model formulations are exploited, depending on which is most common or most illustrative.

Keywords: Phase-field modeling; Microstructure; Nonequilibrium thermodynamics; Kinetics; Simulation

1. Introduction

Most materials are heterogeneous on the mesoscale. Their microstructure consists of grains or domains, which differ in structure, orientation and chemical composition. The physical and mechanical properties on the macroscopic scale highly depend on the shape, size and mutual distribution of the grains or domains. It is, therefore, extremely important to gain insight in the mechanisms of microstructure formation and evolution. However extensive theoretical and experimental research are hereto required, as microstructure evolution involves a large diversity of often complicated processes. Moreover, a microstructure is inherently a thermodynamic unstable structure that evolves in time. Within this domain, the phase-field method has become a powerful tool for simulating the microstructural evolution in a wide variety of material processes, such as solidification, solid-state phase transformations, precipitate growth and coarsening, martensitic transformations and grain growth.

The microstructures considered in phase-field simulations typically consist of a number of grains. The shape and mutual distribution of the grains is represented by functions that are continuous in space and time, the phase-field variables. Within the grains, the phase-field variables have nearly constant values, which are related to the structure, orientation and composition of the grains. The interface between two grains is defined as a narrow region where the phase-field variables gradually vary between their values in the neighboring grains. This modeling approach is called a diffuse-interface description. The evolution of the shape of the grains, or in other words the position of the interfaces, as a function of time, is implicitly given by the evolution of the phase-field variables.

An important advantage of the phase-field method is that, thanks to the diffuse-interface description, there is no need to track the interfaces (to follow explicitly the position of the interfaces by means of mathematical equations) during microstructural evolution. Therefore, the evolution of complex grain morphologies, typically observed in technical alloys, can be predicted without making any a priori assumption on the shape of the grains. The temporal evolution of the phase-field variables is described by a set of partial differential equations, which are solved numerically. Different driving forces for microstructural evolution, such as a reduction in bulk energy, interfacial energy and elastic energy, can be considered. The phase-field method has a phenomenological

* Corresponding author. Tel.: +32 16 321278; fax: +32 16 321991.
E-mail address: nele.moelans@mtm.kuleuven.be (N. Moelans).
URL: http://nele.studentenweb.org (N. Moelans).

0364-5916/$ - see front matter © 2007 Elsevier Ltd. All rights reserved.
doi:10.1016/j.calphad.2007.11.003

character: the equations for the evolution of the phase-field variables are derived based on general thermodynamic and kinetic principles; however, they do not explicitly deal with the behavior of the individual atoms. As a consequence, material specific properties must be introduced into the model through phenomenological parameters that are determined based on experimental and theoretical information.

Nowadays, the phase-field technique is very popular for simulating processes at the mesoscale level. The range of applicability is growing quickly, amongst other reasons because of increasing computer power. Besides solidification [1] and solid-state phase transformations [2], phase-field models are applied for simulating grain growth [3], dislocation dynamics [4–6], crack propagation [7,8], electromigration [9], solid-state sintering [10–12] and vesicle membranes in biological applications [13,14]. In current research, much attention is also given to the quantitative aspects of the simulations, such as parameter assessment and computational techniques.

The aim of the paper is to give a comprehensive introduction to phase-field modeling. The basic concepts are explained and illustrated with examples from the literature to show the possibilities of the technique. Numerous references for further reading are indicated.

2. Historical evolution of diffuse-interface models

More than a century ago, van der Waals [15] already modeled a liquid–gas system by means of a density function that varies continuously at the liquid–gas interface. Approximately 50 years ago, Ginzburg and Landau [16] formulated a model for superconductivity using a complex valued order parameter and its gradients, and Cahn and Hilliard [17] proposed a thermodynamic formulation that accounts for the gradients in thermodynamic properties in heterogeneous systems with diffuse interfaces. The stochastic theory of critical dynamics of phase transformations from Hohenberg and Halperin [18] and Gunton et al. [19] also results in equations that are very similar to the current phase-field equations. Nevertheless, the concept of diffuse interfaces was introduced into microstructural modeling only 20 years ago. There are essentially two types of phase-field model that have been developed independently by two communities.

The first type of phase-field model was derived by Chen [20] and Wang [21] from the microscopic theory of Khachaturyan [22,23]. The phase-field variables are related to microscopic parameters, such as the local composition and long-range order parameter fields reflecting crystal symmetry relations between coexisting phases. The model has been applied to a variety of solid-state phase transformations (see [2] for an overview) that involve a symmetry reduction, for example the precipitation of an ordered intermetallic phase from a disordered matrix [24–26] and martensitic transformations [27,28]. It was also applied to ferroelectric [29,30] and magnetic domain evolution [31] and can account for the influence of elastic strain energy on the evolution of the microstructure. The group of Chen at Pennsylvania State University (USA), the group of Wang at Ohio State University (USA) and the group of Khachaturyan at Rutgers University (USA) are leading within this phase-field community. Similar phase-field models are used by Miyazaki [32,33] (Nagoya Institute of Technology, Japan) and Onuki and Nishimori [34] (Kyoto University, Japan) to describe spinodal decomposition in materials with a composition-dependent molar volume and by Finel and Le Bouar (ONERA, France) for describing the interaction of stress, strain and dislocations with precipitate growth and structural phase transitions [5,35,36].

In the second type of phase-field model, a phenomenological phase-field is used purely to avoid tracking the interface. The idea was introduced by Langer [37] based on one of the stochastic models of Hohenberg and Halperin [18]. The model is mainly applied to solidification, for example to study the growth of complex dendrite morphologies, the microsegregation of solute elements and the coupled growth in eutectic solidification (see [1,38] for an overview). Important contributions were, amongst others, due to Caginalp (University of Pittsburgh, USA) [39,40], Penrose and Fife [41], Wang and Sekerka [42], Kobayashi [43], Wheeler, Boettinger and McFadden (NIST, USA and University of Southampton, UK) [44–48], Kim and Kim (Kunsan National University and Chongju University, Korea) [49], Karma (Northeastern University, USA) and Plapp (Ecole Polytechnique, France) [50–54] and at the Royal Institute of Technology (Sweden) [55–57]. Multiphase-field models for systems with more than two coexisting phases were formulated by Steinbach et al. [58,59] (Access, Germany) and Nestler (Karlsruhe University of Applied Sciences, Germany), Garcke and Stinner (University of Regensburg, Germany) [60,61]. Vector-valued phase-field models in which the phase-field is combined with an orientation field for representing different crystal or grain orientations have been developed by Kobayashi (Hokkaido University, Japan), Warren (NIST, USA) and Carter (MIT, USA) [62,63] and by Gránásy et al. (Research institute for solid state physics and optics, Hungary) [64].

3. Sharp-interface versus diffuse-interface models

There is a wide variety of phase-field models, but common to all is that they are based on a diffuse-interface description. The interfaces between domains are identified by a continuous variation of the properties within a narrow region (Fig. 1a), which is different from the more conventional approaches for microstructure modeling as for example used in DICTRA.[1]

In conventional modeling techniques for phase transformations and microstructural evolution, the interfaces between different domains are considered to be infinitely sharp (Fig. 1b), and a multi-domain structure is described by the position of the interfacial boundaries. For each domain, a set of differential equations is solved along with flux conditions and constitutive laws at the interfaces. For example, in the case of diffusion controlled growth of one phase α at the expense of another phase β,

[1] Software for simulating DIffusion Controlled phase TRAnsformations from Thermo-Calc Software (http://www.thermocalc.se).

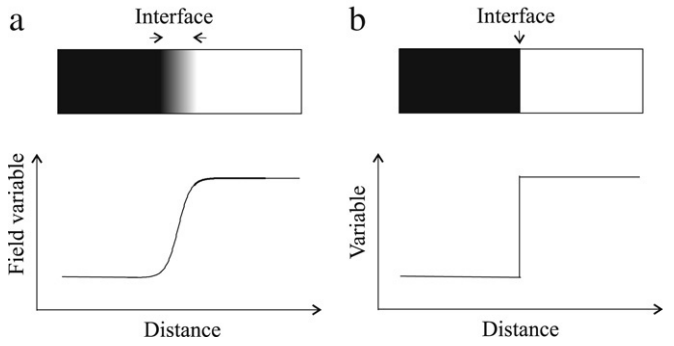

Fig. 1. (a) Diffuse interface: properties evolve continuously between their equilibrium values in the neighboring grains. (b) Sharp interface: properties are discontinuous at the interface.

a diffusion equation for the solute concentration c (mol/m^3) is solved in each phase domain

$$\frac{\partial c^\alpha}{\partial t} = D^\alpha \nabla^2 c^\alpha, \quad \text{for phase } \alpha \tag{1}$$

$$\frac{\partial c^\beta}{\partial t} = D^\beta \nabla^2 c^\beta, \quad \text{for phase } \beta \tag{2}$$

subject to a flux balance that expresses solute conservation at the interface

$$(c^{\alpha,\text{int}} - c^{\beta,\text{int}}) = D^\beta \frac{\partial c^\beta}{\partial r_1} - D^\alpha \frac{\partial c^\alpha}{\partial r_1} \tag{3}$$

and the constitutional requirement that both phases are in thermodynamic equilibrium at the interface

$$\mu^\alpha(c^{\alpha,\text{int}}) = \mu^\beta(c^{\beta,\text{int}}). \tag{4}$$

c^α and c^β are the molar concentrations of the solute element in respectively the α-phase and the β-phase, D^α and D^β the diffusion coefficients and $c^{\alpha,\text{int}}$ and $c^{\beta,\text{int}}$ the molar concentrations at the interface. μ^α and μ^β represent the chemical potentials of the solute for respectively the α-phase and the β-phase. r_1 is the spatial coordinate along the axis perpendicular to the interface. This sharp-interface methodology requires explicit tracking of the moving interface between the α-phase and the β-phase, which is extremely difficult from a mathematical point of view for the complex grain morphologies in real alloys. Sharp-interface simulations are mostly restricted to one-dimensional systems or simplified grain morphologies that, for example, consist of spherical grains.

In the diffuse-interface approach, the microstructure is represented by means of a set of phase-field variables that are continuous functions of space and time. Within the domains, the phase-field variables have the same values as in the sharp-interface model (see Fig. 1a). However, the transition between these values at interfaces is continuous. The position of the interfaces is thus implicitly given by a contour of constant values of the phase-field variables and the kinetic equations for microstructural evolution are defined over the whole system. Using a diffuse-interface description, it is possible to predict the evolution of complex grain morphologies as well as a transition in morphology, like the splitting or coalescence of precipitates and the transition from cellular to dendritic growth in solidification. Furthermore, no constitutional relations of the form (4) are imposed at the interfaces. Therefore, non-equilibrium effects at the moving interfaces, like solute drag and solute trapping, can be studied as a function of the velocity of the interface. Flux conditions are implicitly considered in the kinetic equations.

4. Phase-field variables

In the phase-field method, the microstructural evolution is analyzed by means of a set of phase-field variables that are continuous functions of time and spatial coordinates. A distinction is made between variables related to a conserved quantity and those related to a non-conserved quantity. Conserved variables are typically related to the local composition. Non-conserved variables usually contain information on the local (crystal) structure and orientation. The set of phase-field variables must capture the important physics behind the phase transformation or coarsening process. Since redundant variables increase the computational requirements, the number of variables is also best kept minimal.

4.1. Composition variables

Composition variables like molar fractions or concentrations are typical examples of conserved properties, since the number of moles of each component in the system is conserved. Assume a system with C components and $n_i, i = 1 \ldots C$, the number of moles of each component i. Then the molar fraction x_i and molar concentration c_i (mol/m^3) of component i are defined as

$$x_i = \frac{n_i}{n_{\text{tot}}} \tag{5}$$

and

$$c_i = \frac{n_i}{V} = \frac{x_i}{V_\text{m}}, \tag{6}$$

where $n_{\text{tot}} = \sum n_i$ is the total number of moles in the system, V_m the molar volume and V the total volume of the system. At each position $\overrightarrow{r}$ in the system

$$\sum_{i=1}^{C} x_i = 1 \quad \text{en} \quad \sum_{i=1}^{C} c_i = \frac{n_{tot}}{V} = \frac{1}{V_\text{m}}. \tag{7}$$

As a consequence, the composition field is completely defined by $C - 1$ molar fraction fields $x_i(\overrightarrow{r})$, or $C - 1$ molar concentration fields $c_i(\overrightarrow{r})$ in combination with the molar volume V_m. Since in a closed system the total number of moles of each component is conserved, the temporal evolution of each molar fraction field $x_i(\overrightarrow{r})$ or concentration field $c_i(\overrightarrow{r})$ is restricted by the integral relation

$$\int_V c_i \mathrm{d}\overrightarrow{r} = \frac{1}{V_\text{m}} \int_V x_i \mathrm{d}\overrightarrow{r} = n_i = \text{ct}. \tag{8}$$

Changes in local composition can only occur by fluxes of atoms between neighboring volume elements. Other composition variables are mass fraction or mass per cent.

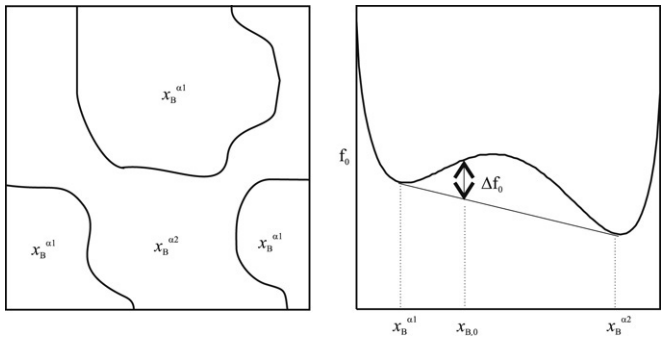

Fig. 2. Representation of a microstructure consisting of two types of domain with different composition, using a single molar fraction field $x_B(\vec{r})$. The free energy density as a function of composition $f_0(x_B)$ has a concave part. Therefore, for a mean composition $x_{B,0}$ in between $x_B^{\alpha 1}$ and $x_B^{\alpha 2}$, the system decomposes into two types of domain, one with composition $x_B^{\alpha 1}$ and the other with composition $x_B^{\alpha 1}$, in order to reduce its free energy content. The compositions $x_B^{\alpha 1}$ and $x_B^{\alpha 2}$ are determined by the common tangent to the free energy curve, and the free energy of the decomposed system corresponds to the points on the common tangent.

Fig. 2 shows the representation of a microstructure by a single molar fraction field. The structure consists of two types of domain with different compositions $x_B^{\alpha 1}$ and $x_B^{\alpha 2}$. At the interface between two domains, $x_B(\vec{r})$ varies smoothly but localized from $x_B^{\alpha 1}$ to $x_B^{\alpha 2}$. Such a representation was widely used for spinodal decomposition and further coarsening of the decomposed structure [65,34,66,67,32,33] and precipitation and growth of precipitates [68,69] with the same structure as the matrix phase. A representation by means of composition fields only is also applicable for systems containing domains with a different structure, if the microstructural evolution is diffusion controlled. This was for example the case in phase-field simulations for ternary diffusion couples [70] and simulations for the coarsening of tin/lead solders [71,72].

4.2. Order parameters and phase-fields

Order parameters and phase-fields are both non-conserved variables that are used to distinguish coexisting phases with a different structure. Order parameters refer to crystal symmetry relations between coexisting phases. Phase-fields are phenomenological variables used to indicate which phase is present at a particular position in the system.

4.2.1. Order parameters

The concept of order parameters originates from microscopic theories and was introduced in continuous theories by Landau for the description of phase transformations that involve a symmetry reduction [73]. Originally, the Landau theory was developed for the description of second-order phase transformations at a critical temperature T_c.[2] Each phase is represented by a specific value of an order parameter (or combination of values of a set of order parameters). Subsequently, a free energy – or Landau polynomial – is formulated as a function of the order parameters and the temperature. For $T > T_c$ the Landau polynomial has minima at the order parameter values corresponding to the high temperature phase and for $T < T_c$ at the order parameter values corresponding to the low temperature phase. The number of order parameters and the equilibrium values of the order parameters reflect the symmetry relations between the phases.

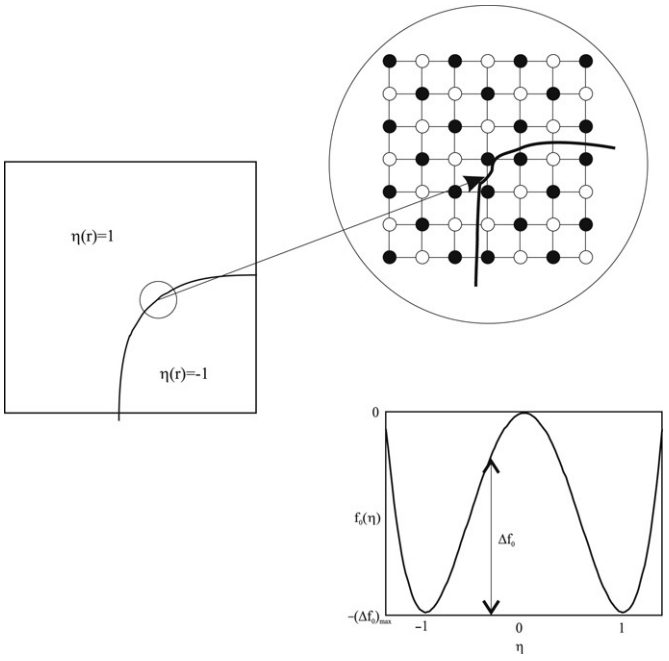

Fig. 3. Two-dimensional representation of an anti-phase structure with cubic symmetry by means of a single order parameter field $\eta(\vec{r})$. The ordered structure consists of two sublattices occupied by a different type of atom, represented by black and white dots. The free energy density as a function of η has a maximum at $\eta = 0$, corresponding to the disordered structure which is unstable, and two minima with equal depth at $\eta = \pm 1$, corresponding to the two equivalent variants of the ordered structure.

In the phase-field models of Chen and Wang and other followers of Khachaturyan's microscopic theory, order parameter fields are mostly used for representing a microstructure. In Fig. 3 is illustrated how a single order parameter field $\eta(\vec{r})$ is used to describe the evolution of an ordered system with anti-phase boundaries in two dimensions [74]. The composition of the alloy is assumed to be constant. As shown in the figure, the ordered structure consists of two sublattices, each occupied by a different type of atom. The atoms can occupy the sublattices in two energetically equivalent ways. The two variants of the ordered phase are distinguished by means of an order parameter η. Within the ordered domains η equals 1 or -1, depending on which sublattice is occupied by which type of atom. $\eta = 0$ corresponds to a disordered phase where the atoms are randomly distributed over the sublattices.

Fig. 4 illustrates the use of order parameters for the description of a phase transformation that involves a symmetry reduction, in this case a cubic to tetragonal phase transformation. The tetragonal phase has a lower symmetry

[2] Since, it has been proven that the Landau theory cannot describe the critical phenomena occurring around T_c for a second-order phase transformation. Nevertheless, statistical theories and experimental facts have confirmed that outside the critical range, the Landau theory is applicable for first- and second-order phase transformations. Especially, the symmetry concepts introduced by Landau are useful.

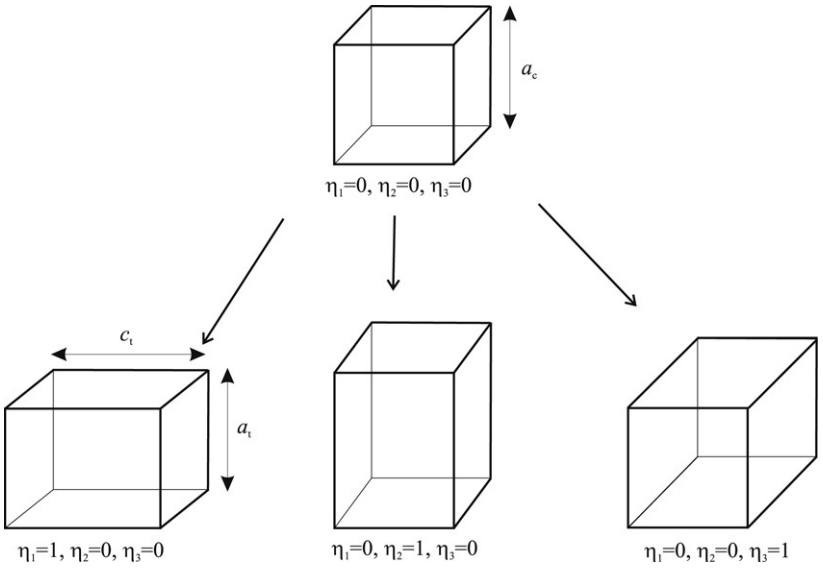

Fig. 4. As a tetragonal structure has less symmetry than a cubic structure, it can be oriented in three equivalent ways with respect to the cubic structure. A set of three order parameter fields is used to distinguish the three tetragonal variants and the cubic phase. a_c, a_t and c_t are the crystal lattice parameters of the cubic and tetragonal phase.

than the cubic phase. Therefore, it can have three orientations that are energetically equivalent (if only chemical energy is considered) and have the same probability to form from the cubic parent phase. Because of the transformation strains associated with a cubic to tetragonal transformation, domains with a different variant of the tetragonal phase interact to reduce elastic strain energy. Therefore, it is relevant to use three order parameters to distinguish the three variants. This representation with three order parameter fields was for example used by Wang [27] for modeling a cubic to tetragonal martensitic transformation.

To model the growth of ordered precipitates or precipitates with a lower symmetry than the matrix phase, a set of order parameter fields is combined with a molar fraction field. The evolution of ordered precipitates with $L1_2$ structure in Ni-based superalloys (fcc structure) was, for example, frequently simulated using a phase-field model [75,24,25,76]. In three dimensions, the ordered $L1_2$ structure consists of four interpenetrating simple cubic lattices which are all equivalent with respect to the fcc disordered matrix phase. The four variants are distinguished by four combinations of three order parameter fields, namely

$$(1,1,1)\eta_{eq},\quad (-1,-1,1)\eta_{eq},\quad (-1,1,-1)\eta_{eq}\quad \text{and}\quad (1,-1,-1)\eta_{eq}.$$

Phase transformations with a more complicated symmetry reduction were also modeled, like the growth of rhombohedral $Ti_{11}Ni_{14}$ precipitates in a cubic TiNi phase [77], the growth of ordered precipitates with tetragonal structure ($L1_0$ structure) in a cubic fcc matrix for Co–Pt and Cu–Au–Pt alloys [35], and structural hexagonal to orthorhombic transformations [78,79].

The order parameter representation was generalized to multi-domain structures by Chen [3,80]. The approach has been used extensively for the study of grain growth [81–87], where the different crystallographic orientations are represented with a large number of order parameter fields $\eta_1, \eta_2, \ldots, \eta_p$. Within each grain one of the field variables equals 1 or -1 and the others equal 0. In this model the order parameter fields are no longer related to crystallographic symmetry variants. They are merely introduced to distinguish between different grains or domains. The effect of solute drag on grain growth [88] and the coarsening of two-phase structures [89,90] were considered as well by adding an additional concentration field to the set of order parameter fields.

There are no restrictions on the evolution of the order parameter fields analogous with relations (7) and (8).

4.2.2. Phase-fields

The concept of a continuous non-conserved phase-field for distinguishing two coexisting phases was introduced by Langer [37]. The phase-field equals 0 in one of the phases and 1 in the other. For example, in the case of solidification

$$\begin{aligned}\phi &= 0 \quad \text{in the liquid}\\ \phi &= 1 \quad \text{in the solid,}\end{aligned} \tag{9}$$

and ϕ varies continuously from 1 to 0 at the solid–liquid interface. Here, ϕ represents the local fraction of the solid phase. The single-phase-field representation in combination with a temperature and/or composition field was extensively applied to study free dendritic growth [43,91–93] in an undercooled melt, cellular pattern formation during directional solidification [53,94] and eutectic growth [47,95]. Non-equilibrium effects such as microsegregation [96] and solute trapping [46,97] could be reproduced in the simulations. The concept of a phase-field was also applied to solid-state phase transformations, like the austenite to ferrite phase transformation in steel (for example $\phi = 1$ in the austenite phase and $\phi = 0$ in the ferrite phase). The transitions between diffusion controlled transformation, Widmanstätten growth and

massive transformation were investigated for an Fe–C alloy [56,98] and an Fe–C–Mn alloy [99].

The single-phase-field formalism was extended towards multiphase systems by Steinbach et al. [58,59]. In a multiphase-field model, a system with p coexisting phases is described by means of p phase-fields ϕ_k, which represent the local fractions of the different phases. Hence, the phase-fields have to sum up to one at every point $\vec{r}$ in the system

$$\sum_{k=1}^{p} \phi_k = 1 \quad \text{with } \phi_k \geq 0, \forall k \tag{10}$$

and only $p-1$ phase-fields are independent in a system containing p coexisting phases. As phase-fields are non-conserved, there are no integral restrictions analogous with relation (8) on the evolution of the phase-fields. The amount of a particular phase is in general not constant in time.

The multiphase-field models provide a general approach for solidification reactions that involve multiple phases, such as eutectic and peritectic solidification [100–102,52]. Besides the general multiphase-field model, models with two [47] or three [101] phase-fields were proposed specifically for eutectic reactions and a model with three phase-fields for coupled two-phase growth in general [54,103]. The multiphase-field model was also applied to grain growth in polycrystalline structures [104] and solid-state phase transformations such as pearlite formation in Fe–C [105,106].

5. Thermodynamic energy functional

The driving force for microstructural evolution is the possibility to reduce the free energy of the system. The free energy F may consist of bulk free energy F_{bulk}, interfacial energy F_{int}, elastic strain energy F_{el} and energy terms due to magnetic or electrostatic interactions F_{fys}

$$F = F_{\text{bulk}} + F_{\text{int}} + F_{\text{el}} + F_{\text{fys}}. \tag{11}$$

The bulk free energy determines the compositions and volume fractions of the equilibrium phases. The interfacial energy and strain energy affect the equilibrium compositions and volume fractions of the coexisting phases, but also determine the shape and mutual arrangement of the domains.

Different from classical thermodynamics where properties are assumed to be homogeneous throughout the system, the free energy F in the phase-field method is formulated as a functional of the set of phase-field variables (which are functions of time and spatial coordinates) and their gradients. When temperature, pressure and molar volume are constant and there are no elastic, magnetic or electric fields, the total free energy of a system defined by a concentration field x_B and a set of order parameter fields η_k, $k = 1 \ldots p$, is for example given by

$$F(x_B, \eta_k) = \int_V f(x_B, \eta_k, \vec{\nabla} x_B, \vec{\nabla} \eta_k) = \int_V \left[f_0(x_B, \eta_k) + \frac{\epsilon}{2} (\vec{\nabla} x_B)^2 + \sum_k \frac{\kappa_k}{2} (\vec{\nabla} \eta_k)^2 \right] \mathrm{d}\vec{r}. \tag{12}$$

$f_0(x_B, \eta_k)$ refers to a homogeneous system where all state variables, in this case the phase-field variables, are constant throughout the system. It is the classical free energy expressed per unit of volume ($\mathrm{J/m^3}$) of a homogeneous system characterized by the local values of the phase-field variables. $f(x_B, \eta_k, \vec{\nabla} x_B, \vec{\nabla} \eta_k)$ is the local free energy density of a heterogeneous system with diffuse interfaces. In the case of classical Gibbsian thermodynamics for heterogeneous (i.e. multiphase) systems with sharp interfaces, the free energy density would correspond to the common tangent to f_0 for the system in Fig. 2 and to the minimum of f_0 for the system in Fig. 3. The gradient terms $(\epsilon/2)\vec{\nabla} x_B$ and $(\kappa_k/2)\vec{\nabla} \eta_k$ are responsible for the diffuse character of the interfaces. ϵ and κ_k are called gradient energy coefficients. They are related to the interfacial energy and thickness. The gradient energy coefficients are always positive, so that gradients in the phase-field variables are energetically unfavorable and give rise to surface tension. This free energy formalism for heterogeneous systems with diffuse interfaces was first introduced by Cahn and Hilliard [17].

The homogeneous free energy density f_0 is a function of the local values of the phase-field variables and reflects the equilibrium bulk conditions of the coexisting domains. With respect to the non-conserved phase-field variables, it has degenerate minima at the values the phase-fields or order parameters can have in the different domains (see for example the free energy function in Fig. 3). For the conserved composition variables, the homogeneous free energy has a common tangent at the equilibrium compositions of the coexisting phases (see for example the free energy function in Fig. 2).

According to Cahn and Hilliard [17], the interfacial energy F_{int} of a system with diffuse interfaces and with a free energy functional of the form (12) is defined as

$$F_{\text{int}}(x_B, \eta_k) = \int_V \left[\Delta f_0(x_B, \eta_k) + \frac{\epsilon}{2} (\vec{\nabla} x_B)^2 + \sum_k \frac{\kappa_k}{2} (\vec{\nabla} \eta_k)^2 \right] \mathrm{d}\vec{r}, \tag{13}$$

where Δf_0 is the difference between the bulk free energy density for the actual local values of the phase-field variables $f_0(x_B, \eta_k)$ and the equilibrium free energy f_{eq} when interfaces are neglected (i.e. the equilibrium free energy according to classical Gibbsian thermodynamics for heterogeneous systems). The meaning of Δf_0 is indicated in Figs. 2 and 3. Minimization of the integral (13) for a planar boundary gives the equilibrium profile of the phase-field variables across an interface and the specific interfacial energy.

Relation (13) shows that, in phase-field models, the interfacial energy F_{int} consists of two contributions: one resulting from the fact that the phase-field variables differ from their equilibrium values at the interfaces, and the other from the fact that interfaces are characterized by steep gradients in the phase-field variables. Within the domains Δf_0 and the gradient terms are equal to zero, since the phase-field variables are constant and have their equilibrium values. Therefore, bulk material does

not contribute to the interfacial energy, as it is supposed to do. The width of the diffuse interfacial regions is the result of two opposing effects. The wider, or the more diffuse, the interfacial region, the smaller the contribution of the gradient energy terms. However, for wider interfaces, there is more material for which the phase-field variables have non-equilibrium values and the integrated contribution from Δf_0 is accordingly larger. Therefore, larger values of the gradient energy coefficients result in more diffuse interfaces, whereas deeper energy wells result in sharper interfaces. For some phase-field formulations, there exist analytical relations between the gradient energy coefficients and the interfacial energy and thickness. In general, however, interfacial energy must be evaluated numerically from an integral equation of the form 13.

Strictly speaking, Gibbs energy should be used in the case of constant temperature and pressure and Helmholtz energy in the case of constant temperature and volume. In many phase-field models, however, pressure and volume are assumed to be constant. Under these restrictions, the Gibbs energy G and Helmholtz energy A only differ by a constant term, since $G = A - pV$. Since

$$\mathrm{d}G = \mathrm{d}A - \mathrm{d}(pV) = \mathrm{d}A + 0, \tag{14}$$

minimization of either of these functions leads to the same conclusions. In general, the free energy F is used to describe the thermodynamic properties of the system in phase-field modeling. It is not always stated clearly whether it refers to Gibbs or Helmholtz energy.

Especially in the formulation of the free energy functional, there are many differences among the phase-field models. In the following sections, a few examples of free energy functionals are given. The models for solid-state phase transformations involving coherency strains, the single-phase-field models and the multiphase-field model are discussed.

5.1. Solid-state phase transformations with symmetry reduction or ordering

The groups of Chen and Wang are specialized in phase-field simulations for solid-state phase transformations involving a symmetry reduction or ordering reaction. It was illustrated in Section 4.2 that these phase transformations can be described by physically well-defined order parameters that are related to the crystal symmetry of the phases. The chemical contribution to the free energy of the system F is of the form (12), where the homogeneous free energy density f_0 is expressed as a Landau polynomial of the order parameters and, if applicable, the composition. To incorporate the elastic energy produced by transformation strains, the standard phase-field model is combined with the micro-elasticity theory of Khachaturyan, which allows us to express the elastic energy as a function of composition and order parameters.

5.1.1. Landau expressions for the homogeneous free energy density

In the following paragraphs, the Landau polynomial is formulated as a function of order parameters and composition for the structures introduced in Section 4.2.

Anti-phase domain structure. By means of the anti-phase domain structure depicted in Fig. 3, it is illustrated how the form of the Landau free energy function is determined. Usually a fourth-order or sixth-order Landau polynomial is used. The most general form of a polynomial of the fourth order for one order parameter is

$$f_0(\eta) = f^{\mathrm{dis}} + A\eta + B\eta^2 + C\eta^3 + D\eta^4. \tag{15}$$

Since both variants of the ordered structure are energetically equivalent, the free energy expression must be symmetric around zero. Hence, all coefficients of uneven terms (A and C) are zero. If it is assumed that the free energy of the disordered phase f^{dis} is equal to zero and the minima are located at $\eta = 1$ and $\eta = -1$, the following free energy expression is obtained:

$$f_0(\eta) = 4(\Delta f_0)_{\max}\left(-\frac{1}{2}\eta^2 + \frac{1}{4}\eta^4\right), \tag{16}$$

where $(\Delta f_0)_{\max}$ is the depth of the free energy. Since the free energy has a maximum at $\eta = 0$, the disordered phase is unstable and will spontaneously evolve towards one of the ordered variants.

Cubic to tetragonal transformation. In the case of the cubic to tetragonal phase transformation in three dimensions depicted in Fig. 4, the Landau free energy as a function of three order parameters must have six minima with equal depth at

$$(\eta_1, \eta_2, \eta_3) = (\pm\eta_{\mathrm{eq}}, 0, 0), (0, \pm\eta_{\mathrm{eq}}, 0), (0, 0, \pm\eta_{\mathrm{eq}}).$$

The value of η_{eq} depends on temperature and composition. Wang and Khachaturyan [27] proposed the following sixth-order expression for a cubic to tetragonal martensitic transformation:

$$f(\eta_1, \eta_2, \eta_3) = \frac{1}{2}A\sum_{k=1}^{3}\eta_i^2 - \frac{1}{4}B\sum_{k=1}^{3}\eta_i^4 + \frac{1}{6}C\left(\sum_{k=1}^{3}\eta_i^2\right)^3, \tag{17}$$

with A, B and C positive constants that determine the value of η_{eq}. Besides the degenerate minima corresponding with the six symmetry variants, it has a local minimum at $(\eta_1, \eta_2, \eta_3) = (0, 0, 0)$ to express the first-order character of the martensitic transformation. Formation of a tetragonal domain within the cubic parent phase involves the formation of stable nuclei to overcome the energy barrier around $(\eta_1, \eta_2, \eta_3) = (0, 0, 0)$.

Precipitation of an ordered intermetallic in a disordered matrix. The following Landau polynomial $f_0(x_B, \eta)$

$$f_0(x_B, \eta) = \frac{1}{2}A(x_B - x_B')^2 + \frac{1}{2}B(x_B'' - x_B)\eta^2 - \frac{1}{4}C\eta^4 + \frac{1}{6}D\eta^6 \tag{18}$$

was proposed by Wang and Khachaturyan [75] for simulating the evolution of ordered precipitates in a disordered matrix for a two-dimensional binary system. A, B, C, D are positive

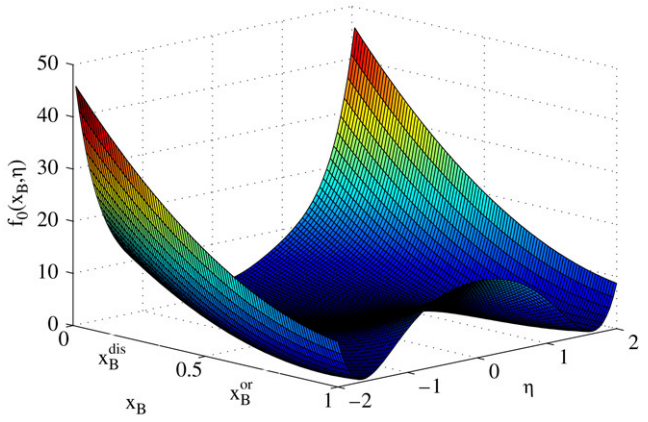

Fig. 5. Landau free energy as a function of one composition variable x_B and one order parameter η as given by relation (18). The parameter values are taken from [75]. With respect to the order parameter, the Landau free energy has a single minimum at $\eta = 0$ for x_B near x_B^{dis} and two degenerate minima symmetrical around zero for x_B near x_B^{or}.

phenomenological constants with a dimension of energy and x'_B and x''_B constants with a dimension of composition. In analogy with the antiphase domain structure in Fig. 3, it was assumed that there are two equivalent variants of the ordered phase, represented by $\eta = \eta_{\text{eq}}$ and $\eta = -\eta_{\text{eq}}$. A three-dimensional view of the free energy density as a function of the order parameter and the molar fraction is shown in Fig. 5. For x_B near x_B^{dis}, $f_0(x_B^*, \eta)$ for constant x_B^*, has a single minimum at $\eta = 0$ corresponding to the disordered matrix phase. For x_B near x_B^{or}, $f_0(x_B^*, \eta)$ has two degenerate minima at $\eta = \pm\eta_{\text{eq}}(x_B^*)$, corresponding to the two variants of the ordered phase. η_{eq} is a function of the composition.

Minimization of the homogeneous free energy density $f_0(x_B, \eta)$ with respect to the order parameter yields the composition dependence of the free energy of a homogeneous system (see the bold curve in Fig. 6a). $f_0(x_B, \eta = 0)$ corresponds to the free energy of the disordered phase. The free energy of the ordered phase must be calculated by replacing η in the Landau polynomial by its equilibrium value $\eta_{\text{eq}}(x_B)$. $\eta_{\text{eq}}(x_B)$ is obtained by minimizing the free energy density for fixed compositions x_B^* (see Fig. 6b). Δf is the driving force for precipitation of the ordered phase in a supersaturated disordered structure with composition $x_{B,0}$. At the diffuse interfacial regions between an ordered and a disordered domain, the concentration and the order parameter are forced to vary continuously between their equilibrium values. Therefore, f_0 is not minimal at the interfaces. The exact evolution of f_0 across an interface depends on the gradient energy coefficients associated with the gradients in the composition and the order parameter. The dotted line in Fig. 6 shows a possible evolution of the homogeneous free energy density across a precipitate–matrix interface. Δf_0 indicates the local contribution to the interfacial energy from the diffuse interfaces.

The phenomenological parameters A, B, C, D must be chosen so that the composition dependence of the equilibrium free energy $f_0(x_B, \eta(x_B))$ agrees with experimental information. Most important is that the driving force for precipitation and the

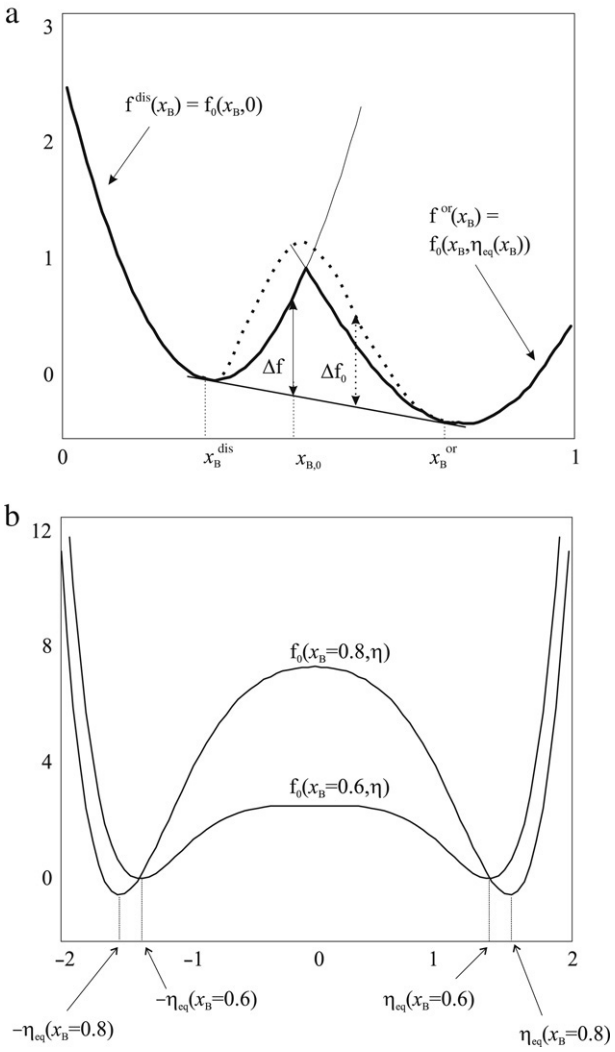

Fig. 6. (a) Minimization of the Landau free energy density (18) with respect to the order parameter yields the composition dependence of the free energy density for a homogeneous system (bold line). Δf is the driving force for precipitation of the ordered phase in a supersaturated disordered structure with composition $x_{B,0}$. The dotted line gives a possible evolution of f_0 across an interfacial region between a precipitate and the matrix. Δf_0 indicates the contribution of the homogeneous free energy density to the interfacial energy in a heterogeneous system. (b) Landau free energy (18) as a function of the order parameter at fixed compositions $x_B = 0.6$ and $x_B = 0.8$.

equilibrium composition of the ordered and disordered phase are reproduced. The exact dependence of the non-equilibrium free energy $f_0(x_B, \eta)$ on the order parameter is not critical as long as the number of minima and the symmetry properties are correctly reproduced.[3]

In the case of the ordered precipitates with $L1_2$ structure in fcc Ni-based superalloys, the Landau free energy polynomial is a function of three order parameters and the composition

[3] The Landau expressions (16)–(18) are, in fact, non-equilibrium free energies, since the free energy at thermodynamic equilibrium only depends on external state variables, such as the composition. The order parameters are so-called internal state variables, which describe internal degrees of freedom in a system that is not in thermodynamic equilibrium [107]. The concept of internal state variables is mainly applied for the description of phase transformations and homogeneous reacting systems.

[24,25,76,26,108]. The coefficients are chosen so that, for compositions near that of the ordered phase, it has four degenerate minima at $(\eta_1, \eta_2, \eta_3) = (1, 1, 1)\eta_{eq}$, $(-1, -1, 1)\eta_{eq}$, $(-1, 1, -1)\eta_{eq}$ and $(1, -1, -1)\eta_{eq}$, and for compositions near that of the disordered phase, it has a single minimum at $(\eta_1, \eta_2, \eta_3) = (0, 0, 0)$.

5.1.2. Interfacial energy

For the anti-phase domain structure in Fig. 3 represented by a single order parameter field, the interfacial energy and width can be calculated analytically [17,74]. In this specific situation, the total free energy of the system has the form

$$F = F_{bulk} + F_{int} = \int_V \left[f_0(\eta) + \frac{\kappa}{2}(\vec{\nabla}\eta)^2 \right] d\vec{r} \tag{19}$$

with f_0 given by relation (16). The specific interfacial energy σ_{int} (J/m^3) is related to the gradient energy coefficient κ and the depth of the minima of the homogeneous free energy $(\Delta f_0)_{max}$ as

$$\sigma_{int} = \frac{4\sqrt{2}}{3}\sqrt{\kappa(\Delta f_0)_{max}} \tag{20}$$

and the interfacial thickness as

$$l = 2\alpha\sqrt{\frac{\kappa}{(\Delta f_0)_{max}}}. \tag{21}$$

The value of α depends on the definition of the thickness of a diffuse interface, as strictly speaking a diffuse interface reaches infinity. For systems with more than one phase-field variable, the interfacial energy must be calculated numerically [26]. It is generally true that the interfacial energy and the width of the profile of the phase-field variables at interfaces increase for larger values of the gradient energy coefficients κ_k and ϵ. If the set of phase-field variables contains composition fields, only the gradient energy coefficients can be adjusted to fit both the interfacial energy and the width, since f_0 is determined by the composition dependence of the chemical free energies of the coexisting phases (see Fig. 6).

Anisotropy in interfacial energy is usually introduced into the free energy through the gradient terms of the order parameter fields, for instance [109,24],

$$F = \int_V \left[f_0(x_B, \eta_k) + \frac{1}{2}\sum_{i,j=1}^{3} \epsilon_{ij}\frac{\partial x_B}{\partial r_i}\frac{\partial x_B}{\partial r_j} + \frac{1}{2}\sum_{k,l=1}^{p}\sum_{i,j=1}^{3} \kappa_{ijkl}\frac{\partial \eta_k}{\partial r_i}\frac{\partial \eta_l}{\partial r_j} \right] d\vec{r} \tag{22}$$

for ordering in fcc alloys (fcc to $L1_2$ structure). The expression was derived from the microscopic theory of Khachaturyan [24]. κ_{ij} is a second-rank tensor. The cross terms with η_k and η_l allow us to distinguish different types of interface depending on the orientation of the neighboring domains [109]. In [110], a free energy expansion with fourth-rank gradient terms was proposed for systems with cubic anisotropy in interfacial energy.

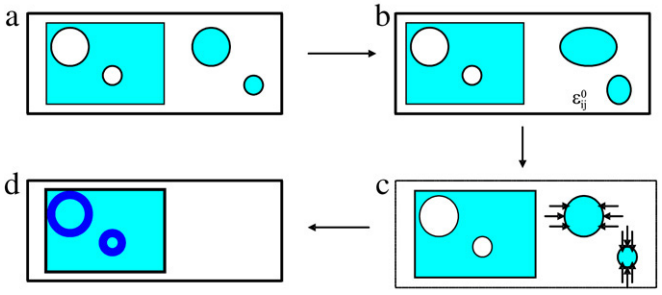

Fig. 7. Successive steps by which a coherent multiphase structure is formed and the associated elastic strain is introduced into the material in micro-elasticity theory (according to Khachaturyan [23]). (a) First the volume elements that will undergo a phase transformation are taken out of the stress-free material. (b) Then, these volume elements are allowed to transform to the new structure at the given temperature and pressure. They will adapt their equilibrium lattice parameters, volume and shape. The strains with respect to the original structure ϵ^0_{ij} are called the stress-free or transformation strains. (c) The transformed volume elements must then be deformed so that they fit again in the system: $\epsilon^{tot}_{ij} = \epsilon^{el}_{ij} + \epsilon^0_{ij} = 0$. After this deformation, elastic strains ($\epsilon^{el}_{ij} = -\epsilon^0_{ij}$) and stresses are present in the transformed material, since its dimensions differ from the equilibrium dimensions. (d) When the transformed material is put back into the system, it can relax to a certain extent: $\epsilon^{el}_{ij} \neq -\epsilon^0_{ij}$. As a consequence, elastic strains and stresses develop in the surrounding material.

5.1.3. Elastic misfit energy

Solid-state phase transformations usually induce elastic stresses into the material that may have a dominant effect on the microstructural evolution [111,112]. The size of domains and precipitates results from the competition between interfacial energy and long-range elastic stresses. In the case of isostructural phase transformations, ordering reactions or symmetry reducing phase transformations, the produced microstructures are, at least in the initial stages of the transformation, coherent, i.e. the lattice planes are continuous across the interfaces. The lattice mismatch at interfaces, caused by a difference in crystal lattice parameters, is accommodated by elastic displacements in the surrounding material. The micro-elasticity theory for multiphase alloys of Khachaturyan [23,113,114] is applied to express the free energy contribution due to coherency strains as a function of the phase-field variables. Fig. 7 illustrates schematically how stress-free or transformation strains and elastic stresses in coherent structures are treated in micro-elasticity theory.

To relate the transformation strains $\epsilon^0_{ij}(\vec{r})$ to the local values of the phase-field variables, a linear dependence on the composition fields and a quadratic dependence on the order parameter fields are mostly assumed:

$$\epsilon^0_{ij}(\vec{r}) = \epsilon^{x_B}_{ij}\delta x_B(\vec{r}) + \sum_k \epsilon^{\eta_k}_{ij}\eta^2_k(\vec{r}). \tag{23}$$

$\delta x_B(\vec{r}, t) = x_B(\vec{r}, t) - x_{B,0}$, with $x_{B,0}$ a reference composition, which is for example taken equal to the overall composition of the alloy. $\epsilon^{x_B}_{ij}$ are the lattice expansion coefficients related to the composition. Following Vegard's law,

$$\epsilon^{x_B}_{ij}(\vec{r}) = \frac{1}{a}\frac{da}{dx_B}\delta_{ij} \tag{24}$$

with a the stress-free lattice parameter. The $\epsilon_{ij}^{\eta_k}$ reflect the lattice mismatch between the product and parent phase. For example, for the cubic to tetragonal transformation shown in Fig. 4 and using a coordinate system with axes parallel to the axes of the cubic crystal, they have the form [27]

$$\epsilon^{\eta_1} = \begin{pmatrix} \epsilon_3 & 0 & 0 \\ 0 & \epsilon_1 & 0 \\ 0 & 0 & \epsilon_1 \end{pmatrix} \qquad \epsilon^{\eta_2} = \begin{pmatrix} \epsilon_1 & 0 & 0 \\ 0 & \epsilon_3 & 0 \\ 0 & 0 & \epsilon_1 \end{pmatrix}$$
$$\epsilon^{\eta_3} = \begin{pmatrix} \epsilon_1 & 0 & 0 \\ 0 & \epsilon_1 & 0 \\ 0 & 0 & \epsilon_3 \end{pmatrix}.$$

The stress-free strains ϵ_1 and ϵ_3 are related to the crystal lattice parameters a_c, a_t and c_t of the cubic and tetragonal structure in their stress-free state

$$\epsilon_1 = \frac{a_t - a_c}{a_c \eta_{eq}^2}, \qquad \text{and} \qquad \epsilon_3 = \frac{c_t - a_c}{a_c \eta_{eq}^2}. \tag{25}$$

The cubic structure is taken as the reference structure.

The elastic strain ϵ_{ij}^{el} is the difference between the total strain ϵ_{ij}^{tot} and the stress-free strain ϵ_{ij}^{0}, both measured with respect to the same reference lattice,

$$\begin{aligned} \epsilon_{ij}^{el}(\vec{r}) &= \epsilon_{ij}^{tot}(\vec{r}) - \epsilon_{ij}^{0}(\vec{r}) \\ &= \epsilon_{ij}^{tot}(\vec{r}) - \epsilon_{ij}^{x_B} \delta x_B(\vec{r}) - \sum_k \epsilon_{ij}^{\eta_k} \eta_k^2(\vec{r}). \end{aligned} \tag{26}$$

The local elastic stress is then calculated by applying Hooke's law from linear elasticity theory,

$$\begin{aligned} \sigma_{ij}(\vec{r}) &= C_{ijkl}(\vec{r}) \epsilon_{kl}^{el}(\vec{r}) \\ &= C_{ijkl}(\vec{r})[\epsilon_{kl}^{tot}(\vec{r}) - \epsilon_{kl}^{0}(\vec{r})], \end{aligned} \tag{27}$$

where the Einstein summation convention is applied and $C_{ijkl}(\vec{r})$ are the elements of the elastic modulus tensor. Since coexisting phases have usually different elastic properties, the elastic modulus tensor depends on the phase-field variables. Next, it is assumed that mechanical equilibrium is reached much faster than chemical equilibrium, so that the equation for mechanical equilibrium

$$\frac{\partial \sigma_{ij}}{\partial r_j} = 0 \tag{28}$$

is valid. Solution of Eq. (28) in combination with relation (27), along with the appropriate mechanical boundary conditions, results in the equilibrium elastic strain field that is present in the material after step 4 in Fig. 7.

To simplify the solution of the elasticity equation (28), the total strain $\epsilon_{ij}^{tot}(\vec{r})$ is considered as the sum of a homogeneous strain $\bar{\epsilon}_{ij}$ related to the macroscopic deformation of the system, and the local heterogeneous strain $\delta\epsilon_{ij}(\vec{r})$ [23]:

$$\epsilon_{ij}^{tot}(\vec{r}) = \bar{\epsilon}_{ij} + \delta\epsilon_{ij}(\vec{r}). \tag{29}$$

This treatment is only valid when the heterogeneities in the microstructure are on a much smaller scale than the macroscopic size of the system. The homogeneous strain is defined so that

$$\int_V \delta\epsilon_{ij}(\vec{r}) \mathrm{d}\vec{r} = 0. \tag{30}$$

The heterogeneous strains are related to the local displacements with respect to the homogeneously deformed material $\vec{u}(\vec{r})$ as

$$\delta\epsilon_{kl}(\vec{r}) = \frac{1}{2}\left[\frac{\partial u_k(\vec{r})}{\partial r_l} + \frac{\partial u_l(\vec{r})}{\partial r_k}\right], \tag{31}$$

where u_i denotes the ith component of the displacement vector $\vec{u}$. Efficient methods have been developed to solve the elasticity equations [4,66,115,116] for materials with heterogeneous elastic properties ($C_{ijkl}(\vec{r})$).

Once the elastic strains are obtained, the total elastic energy F_{el} of the system is calculated through the usual expression,

$$F_{el} = \frac{1}{2}\int_V C_{ijkl}(\vec{r}) \epsilon_{ij}^{el} \epsilon_{kl}^{el} \mathrm{d}\vec{r} \tag{32}$$

for a system under an applied strain $\bar{\epsilon}_{ij}^{a} = \bar{\epsilon}_{ij}$. In the presence of an externally applied stress $\sigma_{ij}^{a}(\vec{r})$, the elastic energy contribution should include the external work [25],

$$F_{el} = \frac{1}{2}\int_V C_{ijkl}(\vec{r}) \epsilon_{ij}^{el} \epsilon_{kl}^{el} \mathrm{d}\vec{r} - \int_V \sigma_{ij}^{a}(\vec{r}) \bar{\epsilon}_{ij}(\vec{r}) \mathrm{d}\vec{r}. \tag{33}$$

The homogeneous strain is then obtained by minimizing the elastic strain energy with respect to the homogeneous strain.

The phase-field micro-elasticity model was applied to a variety of mesoscale phenomena in solid materials. The influence of the elastic properties of the coexisting phases on the morphological evolution in spinodal decomposition and further coarsening of the structure were studied many times [65,34,32,33,21,66,117]. The model also allows us to predict the shape and size of coherent precipitates, as well as the splitting and coalescence of precipitates under influence of an applied stress [77,118,24,25,108,4,76]. For martensitic transformations [27,28,119] and other structural transformations [35,79], the effect of the coherency stresses on the shape and spatial distribution of the different orientation variants were analyzed, as well as the influence of externally applied stresses on the structure. Furthermore, a phase-field micro-elasticity model for the evolution of structures with voids and cracks under an applied stress was proposed [7]. The micro-elasticity formalism was also extended towards polycrystalline materials containing multiple grains with a different orientation [119–121].

Although dislocations are crystal defects on the atomic scale, the stresses they cause on the mesoscale and their effect on microstructural evolution can be modeled using the phase-field micro-elasticity approach. It was possible to reproduce solute segregation (formation of Cottrell atmospheres) and nucleation and growth of precipitates around dislocation cores [4,122]. Furthermore, the interaction between a moving dislocation loop and an array of precipitates [5] was simulated. The movement and multiplication and annihilation of dislocations under an applied stress [6,123] and the formation of dislocation

networks and substructures [124] were also studied by phase-field simulations. Up to now, most micro-elasticity models involving dislocations were for fcc crystals.

When transformation strains are involved, the molar volume is not constant. Nevertheless, Eq. (12) for the chemical free energy is still valid, if considered in a number fixed frame[4] with a constant reference molar volume V_m^{ref}, i.e.

$$F(x_B, \eta_k) = \int_{V^{\text{ref}}} \left[\frac{f_{0,\text{m}}(x_B, \eta_k)}{V_{\text{m}}^{\text{ref}}} + \frac{\epsilon'}{2}(\vec{\nabla} x_B)^2 + \sum_k \frac{\kappa_k'}{2}(\vec{\nabla} \eta_k)^2 \right] \mathrm{d}\vec{r}, \quad (34)$$

where $f_0 = f_{0,\text{m}}/V_{\text{m}}^{\text{ref}}$ and $V^{\text{ref}} = V_{\text{m}}^{\text{ref}} n_{\text{tot}}$, with n_{tot} the total number of moles. $V_{\text{m}}^{\text{ref}}$ is the molar volume of a reference structure, which must be the same as the structure referred to in Eq. (23) and Eqs. (25) for the formulation of the stress-free strains. $f_{0,\text{m}}$ is the homogeneous free energy, expressed per number of moles, assuming the equilibrium lattice parameters at the given temperature and pressure. The free energies f_0 considered up to here are, in fact, of the form $f_0 = f_{0,\text{m}}/V_{\text{m}}^{\text{ref}}$.

An approach similar to that of the elastic strain energy is applied to calculate the electrostatic or magnetic energy contribution when charged species or electric or magnetic dipoles are involved. It is assumed that electric and magnetic equilibrium are much faster than chemical equilibrium. Therefore, an electromagnetic equilibrium equation is first solved to obtain the electric or magnetic field for the current distribution of charges and dipoles and then the total electrostatic or magnetic energy is expressed as a functional of the phase-field variables. To characterize ferroelectric or ferromagnetic domain growth, the order parameter fields are taken equal to the coordinates of the polarization vector for ferroelectric materials [125,29,30] or the coordinates of the magnetization vector for ferromagnetic materials [31].

Recently, elastoplastic phase-field models were proposed by Guo et al. [126] and Hu et al. [127]. Additional phase-field variables are used to describe the plastic strain fields on the mesoscale. The local strain tensor $\epsilon_{ij}^{\text{tot}}$ then consists of an elastic part $\epsilon_{ij}^{\text{el}}$, a contribution due to lattice mismatches ϵ_{ij}^{0}, and a plastic part $\epsilon_{ij}^{\text{pl}}$. Moreover, besides the general terms in the free energy, a distortion strain energy is formulated as a function of the additional phase-field variables for the plastic strain.

5.2. Single-phase-field model for solidification

In the more phenomenologically oriented phase-field models, such as those for solidification, a phase-field ϕ is used to distinguish two coexisting phases. The following functional is an example of a free energy expression used in simulations for isothermal solidification of a single phase from a binary liquid: [46]

$$F = \int_V \left[f_0(x_B, \phi, T^*) + \frac{\epsilon}{2}(\vec{\nabla} x_B)^2 + \frac{\kappa}{2}(\vec{\nabla}\phi)^2 \right] \mathrm{d}\vec{r}, \quad (35)$$

with $f_0(x_B, \phi, T^*)$ the homogeneous free energy density at a given temperature. In many solidification models, the gradient in composition is not considered, i.e. $\epsilon = 0$. The molar volume is usually assumed to be constant.

5.2.1. Homogeneous free energy density

In the single-phase-field model, the homogeneous free energy density consists of an interpolation function $f_p(x_B, \phi, T^*)$ and a double-well function $wg(\phi)$:

$$f_0(x_B, \phi, T^*) = f_{\text{p}}(x_B, \phi, T^*) + wg(\phi). \quad (36)$$

The double-well potential $g(\phi)$

$$g(\phi) = \phi^2(1-\phi)^2 \quad (37)$$

has minima at 0 and 1 and w is the depth of the energy wells. w is either a constant [49] or depends linearly on the molar fraction, namely $w = (1 - x_B)w_A + x_B w_B$ [44]. The interpolation function f_{p} combines the free energy expressions of the coexisting phases $f^\alpha(x_B, T^*)$ and $f^\beta(x_B, T^*)$ into one free energy expression, which is a function of the field variables x_B and ϕ, using a weight function $p(\phi)$:

$$f_{\text{p}}(x_B, \phi, T^*) = (1 - p(\phi)) f^\alpha(x_B, T^*) + p(\phi) f^\beta(x_B, T^*). \quad (38)$$

In this expression, it is assumed that ϕ equals 1 in the β-phase and 0 in the α-phase. The functions $f^\alpha(x_B, T^*)$ and $f^\beta(x_B, T^*)$ are homogeneous free energy expressions for the composition and temperature dependence of the α-phase and the β-phase (see Fig. 8). They are usually constructed, using a regular substitutional solution model or taken from a thermodynamic CALPHAD (CALculation of PHAse Diagrams) description of the phase diagram.

$p(\phi)$ is a smooth function that equals 1 for $\phi = 1$ and 0 for $\phi = 0$ and has local extrema at $\phi = 0$ and $\phi = 1$. Mostly, the following function [42]

$$p(\phi) = \phi^3(6\phi^2 - 15\phi + 10) \quad (39)$$

is used, for which $p'(\phi) = 30g(\phi)$. The functions $g(\phi)$ and $p(\phi)$ are plotted in Fig. 9.

Fig. 10 gives a three-dimensional view of f_0 as a function of x_B and ϕ, obtained from relations (36) and (38) with $w = 1$ and for the free energies of the α-phase and β-phase plotted in Fig. 8. Minimization of f_0 with respect to ϕ at a fixed composition x_B^*, gives $f^\alpha(x_B^*, T^*)$ and $\phi = 0$ or $f^\beta(x_B^*, T^*)$ and $\phi = 1$, depending on which is the lower. The minima correspond with the lower envelope in the projection of f_0 on the $x_B - f_0$-plane shown in Fig. 11a. Thus, in a two-phase structure, ϕ equals 0 in the α-domains and 1 in the β-domains and the free energy equals, respectively, $f^\alpha(x_B^\alpha)$ and $f^\beta(x_B^\beta)$. However, at the diffuse interfaces, ϕ is forced to take values in

[4] This involves that the spatial coordinates expressed in a reference frame related to the physical dimensions of the system are transformed to a reference frame that is defined so that the number of atoms per unit volume of the new reference frame is constant.

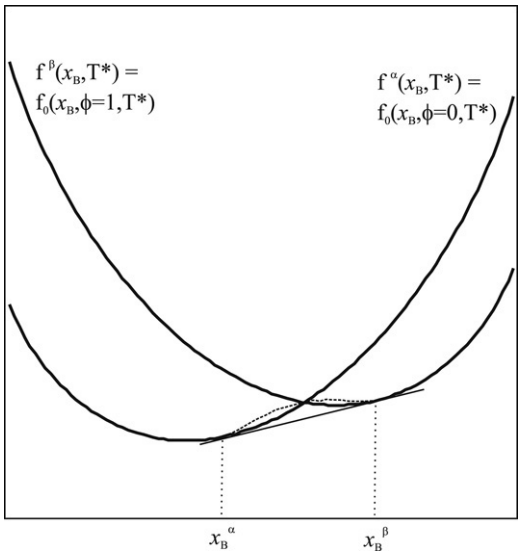

Fig. 8. Phenomenological free energy densities of the phases α and β as a function of composition x_B and at temperature T^*. According to Gibbsian thermodynamics, the system decomposes into two phases for systems with a mean composition $x_{B,0}$ between x_B^α and x_B^β, namely α with composition x_B^α and β with composition x_B^β. The equilibrium compositions of the coexisting phases are given by the tangent rule. The dotted line indicates the evolution of the interpolation function across a diffuse interface.

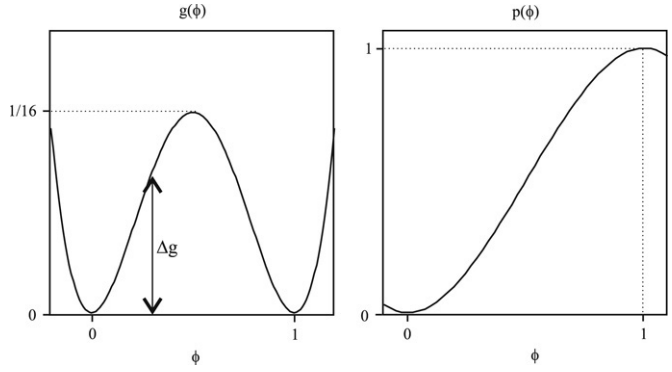

Fig. 9. Double-well potential $g(\phi)$ and weight function $p(\phi)$ used to construct the homogeneous free energy density f_0 for a two-phase system.

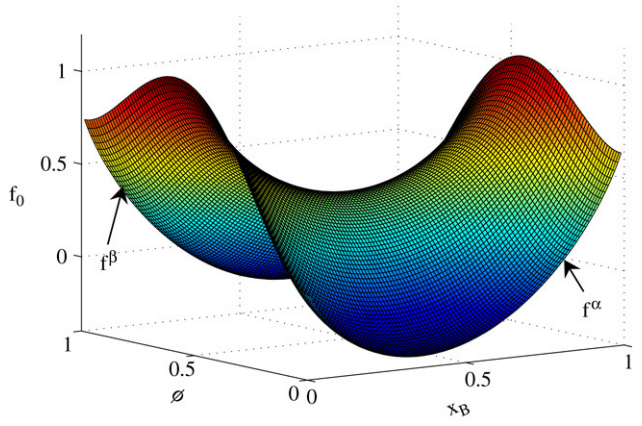

Fig. 10. Three-dimensional graphic of the homogeneous free energy f_0 of a two-phase system according to Eq. (36).

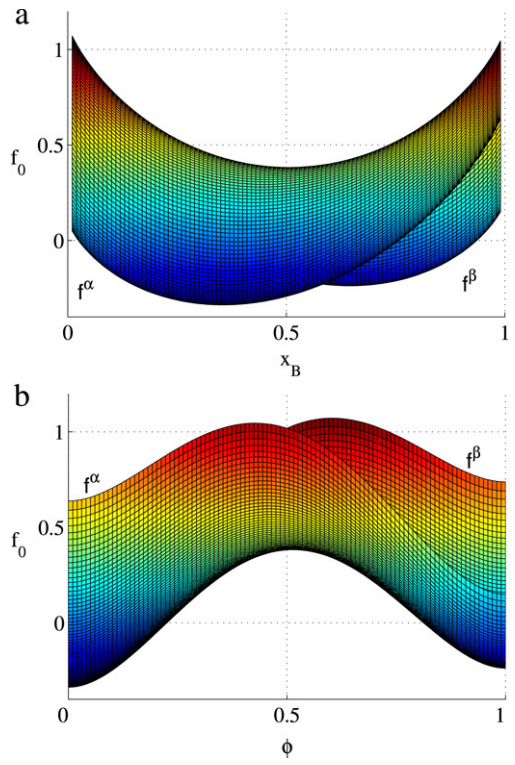

Fig. 11. (a) Projection of f_0 on the x_B–f_0-plane. For homogeneous systems, minimization of the interpolation function f_p with respect to ϕ gives $f_{p,0}(x_B, T^*) = \min(f^\alpha(x_B, T^*), f^\beta(x_B, T^*))$. The lower envelope gives for fixed values of x_B the minimum of f_0 with respect to ϕ. (b) Projection of f_0 on the ϕ–f_0-plane. The lower envelope gives for fixed values of ϕ, the minimum of f_0 with respect to x_B.

between 0 and 1. Then $g(\phi) \neq 0$ and the interpolation function $f_p(x_B^*, \phi, T^*)$ deviates respectively from $f^\alpha(x_B^*, \phi, T^*)$ and $f^\beta(x_B^*, \phi, T^*)$. The dotted line in Fig. 8 indicates how f_p may evolve across a diffuse interface between the α-phase and the β-phase. When $\epsilon = 0$ in the free energy density f (35), the evolution of f_0 across a diffuse interface is given by the minima of f_0 with respect to x_B for fixed values of ϕ. It corresponds to the lower envelope in a projection of f_0 on the ϕ–f_0-plane, which is shown in Fig. 11b.

5.2.2. *Interfacial energy*

In general, the gradient terms, the double-well function $wg(\phi)$ and the interpolation function $f_p(x_B, \phi)$ contribute to the interfacial energy. The contribution from the double-well potential is $w\Delta g$, with Δg as indicated in Fig. 9. The contribution from the interpolation function Δf_p is given by the difference between the dotted line and the common tangent line in Fig. 8. In addition to the gradient energy coefficients, the double-well coefficient w can be modified to adjust the interfacial energy and width. The interfacial energy and width are larger for larger values of the gradient energy coefficients. The interfacial energy increases and the interfacial thickness decreases with the depth of the double-well potential, which is proportional to w. However, there is no analytical relation between the parameters in the phase-field model and the interfacial energy and width [46]. Moreover, the width of the

profile of the concentration variable may differ from that of the phase-field.

In the model of Tiaden et al. [59] and Kim et al. [49], the gradient in concentration is not included in the free energy density, the parameter w in front of the double-well is a constant and an extra restriction is imposed on the local concentration at the interfaces, namely

$$x_B = (1 - p(\phi))\widetilde{x_B^{\alpha}} + p(\phi)\widetilde{x_B^{\beta}} \tag{40}$$

and

$$\frac{\partial f_0}{\partial x_B}(\widetilde{x_B^{\alpha}}) = \frac{\partial f_0}{\partial x_B}(\widetilde{x_B^{\beta}}). \tag{41}$$

They consider the interface as a mixture of two phases with different composition (phase α with composition $\widetilde{x_B^{\alpha}}$ and phase β with composition $\widetilde{x_B^{\beta}}$) and impose that the chemical potential in both phases must be the same. $\widetilde{x_B^{\alpha}}$ and $\widetilde{x_B^{\beta}}$ may differ from the equilibrium bulk compositions x_B^{α} and x_B^{β} indicated in Fig. 8. As a consequence, the interpolation function f_p follows the common tangent line at the interfaces and consequently does not contribute to the interfacial energy. Then, the interfacial energy and thickness only depend on the gradient term in ϕ and the double-well potential. They can be calculated analytically, giving

$$\sigma_{\text{int}} = \frac{\sqrt{\kappa w}}{3\sqrt{2}} \tag{42}$$

and

$$l = \alpha\sqrt{2}\sqrt{\frac{\kappa}{w}}, \tag{43}$$

where α depends on the definition of the interfacial thickness. The advantage of such a model is that the parameters w and κ in the phase-field model are in a straightforward way related to physical properties σ_{int} and l.

5.2.3. Anisotropy

The interfacial energy of a solid–liquid interface may depend on the orientation of the crystal with respect to the interface. Also in the case of solid–solid phase transformations, there are usually low-energy interface orientations resulting in, for example, plate-like particles. To obtain realistic simulations, this anisotropy is included into the phase-field model by giving $\sqrt{\kappa}$ the same orientation dependence as the interfacial energy, as the interfacial energy is proportional to $\sqrt{\kappa}$.

For two-dimensional systems, the normal to the interface $\vec{n} = (n_1, n_2)$, which is in fact the normal to contours of constant value of a phase-field variable ϕ, is given by

$$(n_1, n_2) = \frac{1}{\sqrt{\left(\frac{\partial\phi}{\partial r_1}\right)^2 + \left(\frac{\partial\phi}{\partial r_2}\right)^2}}\left(\frac{\partial\phi}{\partial r_1}, \frac{\partial\phi}{\partial r_2}\right), \tag{44}$$

and the angle θ between the normal to the interface and the r_1-axis by

$$\tan(\theta) = \frac{n_2}{n_1} = \frac{\partial\phi/\partial r_2}{\partial\phi/\partial r_1}. \tag{45}$$

For weak anisotropy, the following formulation is commonly applied for two-dimensional systems [45]:

$$\sqrt{\kappa} = \overline{\kappa}(1 + \nu\cos(k\theta)), \tag{46}$$

with $\nu < 1/15$ a measure of the strength of anisotropy and k the order of anisotropy. For example for cubic anisotropy, k equals 4. According to the Gibbs–Thomson condition $\sigma + \mathrm{d}^2\sigma/\mathrm{d}\theta > 0$ (with σ the interfacial energy and θ the orientation of the normal to the interface), ν in Eq. (46) must be smaller than $1/15$.

In order to describe strong anisotropy in interfacial energy, resulting in faceted morphologies, functions with deep cusps at the low-energy orientations are required. Examples of such anisotropy functions, which were used to distinguish the large difference in energy between a coherent and an incoherent interface, are

$$\sqrt{\kappa} = \overline{\kappa}\,(1 + \nu\,(|\sin(\theta)| + |\cos(\theta)|))\,, \tag{47}$$

resulting in square particles [128], and

$$\sqrt{\kappa} = \frac{\overline{\kappa}}{1+\nu}\,(1 + \nu|\cos(\theta)|)\,, \tag{48}$$

resulting in plate-like particles [129,98,130]. The equations must be regularized as described in [128,98] to circumvent the discontinuities in the first derivative. In both cases, ν defines the amplitude of the anisotropy. More functions for $\sqrt{\kappa}(\vec{n})$ or $\sqrt{\kappa}(\theta)$ have been proposed to simulate the growth of faceted crystals [131–133].

A similar approach is used to describe anisotropy in three dimensions [48,134,135], giving for example

$$\sqrt{\kappa} = \overline{\kappa}\left[1 + \nu\left[\cos^4(\theta_1) + \sin^4(\theta_1) \times \left(1 - 2\sin^2(\theta_2)\cos^2(\theta_2)\right)\right]\right] \tag{49}$$

for weak cubic anisotropy, where θ_1 and θ_2 define the orientation of the normal to the interface in three dimensions.

If the energy gradient coefficient κ depends on the orientation of the interface, the interfacial thickness varies along the interface; see for example Eq. (43). In the case of strong anisotropy, these variations in interfacial thickness may result in artifacts, such as enhanced particle coalescence along high-energy interfaces or numerical pinning along low-energy orientations [136]. Therefore, a better approach would be to make both the energy gradient coefficient and the height of the double-well potential orientation dependent in such a way that the orientation dependence of the interfacial energy is reproduced, while the interfacial thickness is constant along the interface.

5.2.4. Non-isothermal solidification

For non-isothermal solidification, a thermodynamic entropy functional should be considered instead of a free energy

functional [41,137,42,138], since the temperature is not prescribed. For example,

$$S = \int_V \left[s_0(e_0, x_B, \phi) - \frac{\epsilon'}{2}(\vec{\nabla} x_B)^2 - \frac{\kappa'}{2}(\vec{\nabla}\phi)^2 \right] \mathrm{d}\vec{r}, \quad (50)$$

where the homogeneous entropy density s_0 depends on the internal energy density e_0, the phase-field and the composition. The internal energy is a function of temperature. The internal energy e_0, Helmholtz energy f_0 and entropy s_0 are related as $e_0 = f_0 + s_0 T$, with T the temperature. At thermodynamic equilibrium the entropy functional S is maximal.

5.3. Multiphase-field model

Multiphase-field models have been developed for the simulation of phase transformations that involve more than two phases, such as eutectic and peritectic solidification. The microstructure is described by a vector ϕ of multiple phase-fields ϕ_k, which represent the local fractions of the different phases. The free energy as a functional of the molar fraction fields $x_i(\vec{r}, t)$ and phase-fields $\phi_k(\vec{r}, t)$ at a fixed temperature T^* usually has the form [58,100,139]

$$F(x_i, \phi, T^*) = \int_V \left[f_p(x_i, \phi, T^*) + g(\phi) + \sum_{j<k}^{p} \left[\frac{\kappa_{jk}}{2} |\phi_j \vec{\nabla}\phi_k - \phi_k \vec{\nabla}\phi_j|^2 \right] \right] \mathrm{d}\vec{r}, \quad (51)$$

where $\kappa_{jk} = \kappa_{kj}$ is the gradient energy coefficient related to the interface between phases j and k. The gradient energy term is formulated in such a way that the properties of each interface can be treated individually. The contribution $f_p(x_i, \phi, T^*)$ is an interpolation function of the homogeneous free energies of the coexisting phases $f^k(x_i, T^*)$:

$$f_p(x_i, \phi, T^*) = \sum_{k=1}^{p} p(\phi_k) f^k(x_i, T^*). \quad (52)$$

The weight functions $p(\phi_k)$ must obey the same requirements as specified for the weight function in the single-phase-field model (Section 5.2.1). $g(\phi)$ is usually formulated as a multi-well potential

$$g(\phi) = \sum_{j<k}^{p} w_{jk} \phi_j^2 \phi_k^2. \quad (53)$$

It is the analogue of the double-well potential in the single-phase-field model. w_{jk} is a symmetric matrix. The elements $w_{jk} = w_{kj}$ are related to the properties of the interface between phases j and k. Gradients in composition are not considered in the free energy functional and the restrictions (40) and (41) are assumed. As a consequence, the energy and width of the interface between phases j and k only depend on the parameters κ_{jk} and w_{jk}:

$$\sigma_{\mathrm{gb},jk} = \frac{\sqrt{\kappa_{jk} w_{jk}}}{3\sqrt{2}} \quad (54)$$

$$l_{jk} = \frac{\sqrt{2\kappa_{jk}}}{\sqrt{w_{jk}}}. \quad (55)$$

Anisotropy of surface energy can be introduced in a similar way as for the single-phase-field models [140].

Garcke, Nestler and Stinner [141,60,142,61] have formulated a multiphase-field model for non-isothermal solidification in multicomponent and multiphase systems. It is based on an entropy functional of the form

$$S(e_0, x_i, \phi) = \int_V \left[s_0(e_0, x_i, \phi) - \left(\epsilon a(\phi, \vec{\nabla}\phi) + \frac{1}{\epsilon} g(\phi) \right) \right] \mathrm{d}\vec{r}. \quad (56)$$

The first term describes the bulk thermodynamic properties. The entropy density s_0 and the internal energy density e_0 are calculated from a Helmholtz energy density function f_0 using the thermodynamic relations $s_0 = -\partial f_0/\partial T$ and $e_0 = f_0 + T s_0$. The Helmholtz energy f_0, itself, has the form (52), where the $f^k(x_i, T^*)$ are constructed using a substitutional solution model. The second term in the entropy functional is related to the interfacial properties. The coefficient ϵ is a measure for the interfacial width. The term $\epsilon a(\phi, \vec{\nabla}\phi)$ accounts for the gradient energy. $a(\phi, \vec{\nabla}\phi)$ is formulated as a function of the expressions $q_{jk} = |\phi_j \vec{\nabla}\phi_k - \phi_k \vec{\nabla}\phi_j|$, so that the properties of different types of interface can be treated independently. A number of functions are proposed for different types and strengths of anisotropy in interfacial energy. The function $g(\phi)$ has a multi-well

$$g(\phi) = 9 \sum_{j<k} \gamma_{jk} \phi_j^2 \phi_k^2 \quad (57)$$

or multi-obstacle

$$g_{ob}(\phi) = \frac{16}{\pi^2} \sum_{j<k} \gamma_{jk} \phi_j \phi_k \quad (58)$$

form. For the multi-obstacle form, relation (58) is applied when $\sum_{k=1}^{p} \phi_k = 1$ and $\phi_k \geq 0, \forall k$. Otherwise $g_{ob}(\phi_k) = +\infty$ is taken. In the ideal case, the parameter γ_{jk} equals the specific entropy of the interface between phases j and k.

Recently, the multiphase-field models were also coupled with elasticity equations [143,106,144].

6. Phase-field equations

In the phase-field method, the temporal evolution of the phase-field variables is given by a set of coupled partial differential equations, one equation for each variable. Except for a few solidification models that are only concerned with reproducing the traditional sharp-interface models, the equations are derived according to the principles of non-equilibrium thermodynamics [145]. They are chosen so that the free energy decreases monotonically and mass is conserved for all components. Numerical solution of the partial differential equations yields the temporal evolution of the phase-field variables, which is a representation of the morphological evolution of the grains or domains in the system.

6.1. Time-dependent Ginzburg–Landau equation

The non-conserved variables $\eta_k(\vec{r},t)$ and $\phi_k(\vec{r},t)$ govern a time-dependent Ginzburg–Landau equation, also referred to as a Allen–Cahn equation. For the order parameter field representation,

$$\frac{\partial \eta_k(\vec{r},t)}{\partial t} = -L_k \frac{\delta F}{\delta \eta_k(\vec{r},t)} = -L_k \left[\frac{\partial f_0}{\partial \eta_k} - \vec{\nabla} \cdot \kappa_k \vec{\nabla} \eta_k \right] \tag{59}$$

is obtained for $k = 1 \ldots p$, where F and f_0 are functions of the conserved and non-conserved field variables as discussed in Section 5.1. L_k and κ_k may depend on the local values of the field variables to introduce anisotropy or composition dependence of the interfacial energy or mobility. In the single-phase-field model, for example in the case of a system represented by a single phase-field variable ϕ and a composition field x_B, the evolution of ϕ is given by

$$\frac{\partial \phi(\vec{r},t)}{\partial t} = -L \frac{\delta F(x_B,\phi)}{\delta \phi(\vec{r},t)} = -L \left[\frac{\partial f_0(x_B,\phi)}{\partial \phi} - \vec{\nabla} \cdot \kappa(\phi) \vec{\nabla} \phi \right], \tag{60}$$

where it is assumed that κ may depend on the phase-field. In the multiphase-field model, the technique of the λ-multiplier is applied to account for restriction (10) on every position in the system:

$$\frac{\partial \phi_k(\vec{r},t)}{\partial t} = -L \frac{\delta F'(x_B,\phi_l)}{\delta \phi_k(\vec{r},t)}, \tag{61}$$

with

$$F' = \int_V \left[f(x_i,\phi_l,T^*) + \lambda \left(\sum_{l=1}^{p} \phi_l - 1 \right) \right] \mathrm{d}V = F + \int_V \left[\lambda \left(\sum_{l=1}^{p} \phi_l - 1 \right) \right] \mathrm{d}V \tag{62}$$

and F and $f(x_i,\phi_l,T^*)$ respectively the total free energy and the free energy density, which are discussed in Section 5.3. Elimination of λ gives

$$\frac{\partial \phi_k(\vec{r},t)}{\partial t} = -\frac{L}{p} \sum_{l=1}^{p} \left(\frac{\delta F}{\delta \phi_k(\vec{r},t)} - \frac{\delta F}{\delta \phi_l(\vec{r},t)} \right), \tag{63}$$

with p the number of phase-fields.

The L and L_k in Eqs. (59), (60) and (63) are positive kinetic parameters, related to the interfacial mobility μ. It was calculated by Allen and Cahn [74], assuming that $l/\rho \ll 1$ with $1/\rho$ the local curvature of the interface and l the interfacial thickness, that the interfacial velocity equals

$$v = L\kappa \left(\frac{1}{\rho} \right) \tag{64}$$

for curvature driven coarsening of the anti-phase domain structure in Fig. 3. In classical sharp-interface theories for curvature driven motion of interfaces, the velocity of an interface is given by

$$v = \mu \sigma_{\mathrm{int}} (1/\rho) = \mu^* (1/\rho), \tag{65}$$

where μ is called mobility and μ^* reduced mobility. Accordingly, the product $L\kappa$ in the phase-field model is equal to the reduced mobility in classical models for interfacial motion, which is a measurable quantity [146]. Notice that, for curvature driven grain boundary movement, the velocity of the interface is not affected by the form of the non-equilibrium free energy density $f_0(\eta)$ (see e.g. Eq. (16)).

Analogous to the anisotropy in interfacial energy (Section 5.2.3), anisotropy in interfacial mobility is introduced by giving L a dependence on the interfacial orientation through the angle θ defined by relation (45) [133].

6.2. Cahn–Hilliard equation

The evolution of conservative phase-field variables, such as the molar fraction field $x_B(\vec{r},t)$, obeys a Cahn–Hilliard equation, for example,

$$\frac{1}{V_m} \frac{\partial x_B(\vec{r},t)}{\partial t} = \vec{\nabla} \cdot M \vec{\nabla} \frac{\delta F(x_B,\eta_k)}{\delta x_B(\vec{r},t)} = \vec{\nabla} \cdot M \vec{\nabla} \left[\frac{\partial f_0(x_B,\eta_k)}{\partial x_B} - \vec{\nabla} \cdot \epsilon \vec{\nabla} x_B(\vec{r},t) \right]. \tag{66}$$

The kinetic parameter M can be a function of the order parameter fields and the composition. The Cahn–Hilliard equation is essentially a diffusion equation of the form

$$\frac{1}{V_m} \frac{\partial x_B(\vec{r},t)}{\partial t} = -\vec{\nabla} \cdot \vec{J}_B, \tag{67}$$

where the diffusion flux $\vec{J_B}$ is given by

$$\vec{J}_B = -M \vec{\nabla} \frac{\delta F}{\delta x_B} = -M \vec{\nabla} \left[\frac{\partial f_0(x_B,\eta_k)}{\partial x_B} - \vec{\nabla} \cdot \epsilon \vec{\nabla} x_B(\vec{r},t) \right]. \tag{68}$$

Mass conservation is accordingly ensured, as well as the flux balance at the interfaces (compare with Eq. (3) in sharp-interface models). The diffusion fluxes are defined in a number fixed reference frame (the number of moles per unit volume in the number fixed reference frame, is constant in time) and the parameter M relates to the interdiffusion coefficient D as

$$M = \frac{V_m D}{\partial^2 G_m / \partial x_B^2}, \tag{69}$$

which gives for an ideal solution

$$M = \frac{D x_B V_m}{RT}. \tag{70}$$

M can also be expressed as a function of the atomic mobilities of the constituting elements M_A and M_B [147],

$$M = \left(\frac{1}{V_m} \right) x_B (1 - x_B)[x_B M_A + (1 - x_B) M_B]. \tag{71}$$

Atomic mobilities are related to tracer diffusion coefficients. If sufficient experimental information is available, expressions for the temperature and composition dependence of the atomic mobilities M_i can be determined using the DICTRA (DIffusion Controlled Transformation) software (see Section 7.1.1). To account for differences in diffusion properties between the coexisting phases and for enhanced grain boundary diffusion, M may depend on the order parameter fields or phase-fields.

6.3. Heat flow and other transport phenomena

Besides diffusion, other transport processes can have a dominant effect on the microstructure. Using the formalism of linear non-equilibrium thermodynamics [145], it is straightforward to extend the standard phase-field model to include phenomena such as heat diffusion, convection and electric current.

6.3.1. Non-isothermal solidification

For non-isothermal solidification [41,137,42,138], the following equations were obtained for an entropy functional S of the form (50):

$$\begin{aligned}\frac{\partial e}{\partial t} &= -\overrightarrow{\nabla}\cdot M_T \overrightarrow{\nabla}\frac{\partial s}{\partial e}\\ &= -\overrightarrow{\nabla}\cdot M_T \overrightarrow{\nabla}\frac{1}{T},\end{aligned} \tag{72}$$

$$\begin{aligned}\frac{\partial \phi}{\partial t} &= L\left[\frac{\partial s}{\partial \phi}+\kappa'\nabla^2\phi\right]\\ &= -L\left[\frac{1}{T}\frac{\partial f}{\partial \phi}-\kappa'\nabla^2\phi\right]\end{aligned} \tag{73}$$

and

$$\begin{aligned}\frac{1}{V_m}\frac{\partial x_B}{\partial t} &= -\overrightarrow{\nabla}\cdot M\overrightarrow{\nabla}\left[\frac{\partial s}{\partial x_B}+\epsilon'\nabla^2 x_B\right]\\ &= \overrightarrow{\nabla}\cdot M\overrightarrow{\nabla}\left[\frac{1}{T}\frac{\partial f}{\partial x_B}-\epsilon'\nabla^2 x_B\right].\end{aligned} \tag{74}$$

The kinetic parameter M_T in the heat equation (72) can be related to the thermal diffusivity. For a constant temperature, Eqs. (73) and (74) are equivalent with the Ginzburg–Landau equation (60) and the Cahn–Hilliard equation (66).

6.3.2. Convection

Compared to purely diffusive transport, convection in the liquid phase enhances the transport of heat and mass during solidification. One of the methodologies to include convection is to combine the phase-field equations with a Navier–Stokes equation where the viscosity depends on the phase-field [57, 148–151]. In this approach, both the solid and liquid phase are treated as a Newtonian viscous fluid with the viscosity of the solid phase several orders of magnitude larger than that of the liquid phase. A full thermodynamic derivation of the equations for mass, energy and momentum conservation and an equation for the evolution of the non-conserved phase-field was given by Anderson et al. [152]. Very recently the phase-field method was also coupled with the lattice Boltzmann method [153], an alternative technique for simulating fluid flow.

6.3.3. Electric current

Brush [154] derived a phase-field model that considers the effect of heat flow and an applied electric current on crystal growth. The model reproduces typical phenomena related to the combination of heat flow and electric current, such as Joule heating, the Thompson effect and the Peltier effect.

6.3.4. Plastic deformation

In phase-field models for elastoplastic deformation, the evolution of the phase-field variables that describe the plastic strain fields is given by time-dependent Ginzburg–Landau equations with the free energy functional equal to the distortion strain energy [126] or given by an objective function based on a yield criterion [127]. In both cases, the kinetic equations for plastic flow are only defined in regions where the effective stress exceeds a critical value given by the yield criterion.

6.4. Stochastic noise term

Stochastic Langevin forces are sometimes added to the phase-field equations to account for the effect of thermal fluctuations on microstructure evolution, for example,

$$\frac{\partial \eta_k(\overrightarrow{r},t)}{\partial t} = -L\frac{\delta F(x_B,\eta_j)}{\delta \eta_k(\overrightarrow{r},t)}+\zeta_k(\overrightarrow{r},t) \tag{75}$$

$$\frac{1}{V_m}\frac{\partial x_B(\overrightarrow{r},t)}{\partial t} = \overrightarrow{\nabla}\cdot M\overrightarrow{\nabla}\frac{\delta F(x_B,\eta_k)}{\delta x_B(\overrightarrow{r},t)}+\psi_B(\overrightarrow{r},t), \tag{76}$$

with $\zeta_k(\overrightarrow{r},t)$ non-conserved and $\psi_B(\overrightarrow{r},t)$ conserved Gaussian noise fields that satisfy the fluctuation–dissipation theorem [18,19]. The local magnitudes of the Langevin noise terms must be scaled appropriately so that the noise in the bulk phases and interfaces in the phase-field simulations can be related quantitatively with temperature fluctuations that are present in real experiments [155].

Mostly, the Langevin terms are used purely to introduce noise at the start of a simulation and are switched off after a few time steps. For example, to initiate precipitation of an ordered phase in a metastable supersaturated disordered matrix or for the onset of dendritic growth in solidification. Gránásy et al. [156,157] employed the Langevin noise terms to simulate the nucleation of crystal seeds in undercooled melts.

7. Quantitative phase-field simulations for alloy development

The early phase-field simulations showed that the phase-field technique is a general and powerful technique for simulating the evolution of complex morphologies. Simulations could give important insights into the role of specific material or process parameters on the pattern formation in solidification and the shape and spatial distribution of precipitates or different orientation domains in solid-state phase transformations. However, the results were rather qualitative and there are two major difficulties that complicate quantitative simulations for real alloys. The phase-field equations contain many phenomenological parameters, which are often difficult

to determine for real alloys. Furthermore, because in real alloys the width of the interfaces is several orders smaller than the microstructural features (dendrites, grains, precipitates) and processes (heat and mass diffusion), massive computer resources are required to resolve the evolution of the phase-field variables at the interfaces appropriately and, at the same time, cover a system with realistic dimensions. Often, simulations are restricted to simplified or model systems and results are affected by artificial boundary effects. To make the phase-field technique attractive for technical applications, in current research much attention is given to the quantitative aspects of the simulations. Different methodologies are applied to determine the parameters and to deal with the inconveniences of the diffuse interfaces. Moreover, advanced numerical solution techniques are proposed and powerful parallel codes are developed.

7.1. Parameter determination

As is the case for all mesoscale and macroscale modeling techniques, the phase-field equations contain a large number of parameters that must be determined in order to introduce the material specific properties for real alloys. The parameters in the homogeneous free energy density determine the equilibrium composition of the bulk domains, the gradient energy coefficients and, if applicable, the double-well coefficient are related to the interfacial energy and width, the kinetic parameter in the Cahn–Hilliard equation is related to diffusion properties and the kinetic parameter in the Ginzburg–Landau equation to the mobility of the interfaces. For solid-state phase transformations, the microelasticity theory requires also the elastic moduli of all coexisting phases. The parameters may show directional, compositional and temperature dependence. In particular, the orientation dependence of the properties is decisive for the morphological evolution. Due to the large number of parameters and also because some properties or dependences are difficult to determine experimentally, parameter assessment for phase-field models is not straightforward. To reduce the dependence on experimental input, the phase-field technique has been combined with the CALPHAD approach for multicomponent alloys and with atomistic calculations.

7.1.1. CALPHAD approach for multicomponent alloys

The CALPHAD (CALculation of PHAse Diagrams) method was originally developed for the calculation of phase diagrams of multicomponent alloys using thermodynamic Gibbs energy expressions. The required Gibbs energy expressions of the different phases are determined by fitting the parameters in a thermodynamic model using experimental information on thermodynamic properties and phase equilibria. The CALPHAD approach provides an efficient and consistent tool for constructing temperature-dependent and composition-dependent Gibbs energy expressions for multicomponent systems. Different thermodynamic solution models were developed to describe the temperature and composition dependences of the free energy, such as the substitutional solution model (atoms can freely mix over all lattice sites) and the sublattice model (atoms are only allowed to mix within distinct sublattices). In the CALPHAD method, expressions for the Gibbs energy for multicomponent systems are constructed through an 'extrapolation from the binary subsystems'. This means that the expressions of the binary systems are combined according to a mathematical model, resulting in a description of the multicomponent system. Deviations from the model are treated using higher-order interactions parameters. When the parameters of the binary system are known, only the higher-order interaction terms must be determined accordingly to obtain the Gibbs energy of the multicomponent system. Thanks to the standardized approach, the work of different researchers can be combined in large-scale international projects for obtaining thermodynamic databases for complex multicomponent alloys. For many industrial alloy systems, such as steels, light (Al–, Ti–, Mg–) alloys, soldering alloys, ceramic materials and slag systems, thermodynamic databases containing expressions for the interaction parameters are available. Furthermore, computer programs, such as Thermo-Calc[5] and Pandat,[6] were developed for the calculation of the phase diagrams and optimization of the parameters in the Gibbs energy expressions.

Within the DICTRA (DIffusion Controlled TRAnsformations) software[7] for the simulation of diffusion controlled phase transformations for multicomponent alloys (based on a sharp-interface model), temperature-dependent and composition-dependent expressions for the atomic mobilities (see Eq. (71)) are obtained in a similar way as the Gibbs energy expressions in the CALPHAD method [147,158]. The parameters are determined using experimentally measured tracer, interdiffusion, and intrinsic diffusion coefficients. Unfortunately, the number of assessed systems in the DICTRA database is rather limited.

In the single-phase-field and multiphase-field models, where the free energy density is constructed as an interpolation function of the free energies of the coexisting phases, the Gibbs energy expressions from CALPHAD databases can be used directly in the phase-field free energy. The phase-field method was for example combined with thermodynamic CALPHAD databases and kinetic DICTRA databases for simulating solidification of ternary Al–Mg–Si-alloys [63] and commercial Mg–Al–Zn and Al–Si–Cu–Mg–Ni alloys [159], the growth of perlite [106], the morphological evolution in Al–Ni–Cr diffusion couples [70,160], Ostwald ripening in Al–Ni–Cr alloys [161], diffusion controlled precipitate growth and dissolution in Ti–Al–V [162] and the growth and coarsening of the intermetallic compound layer in Cu–Sn leadfree solder joints [163,164]. More details on the coupling of phase-field simulations with thermodynamic and phase diagram calculations are explained in [139]. A phase-field simulation software MICRESS[8] has been developed based on

[5] Department of Materials Science and Engineering, KTH, Stockholm.
[6] CompuTherm LLC.
[7] Department of Materials Science and Engineering, KTH, Stockholm.
[8] ACCESS, Aachen.

the multiphase-field model, which is coupled with the Thermo-Calc software for the thermodynamic calculations.

In the case of the Landau free energy expressions, it is more complicated to determine the parameters in the Landau free energy $f(x_i, \eta_{eq}(x_i))$ from the CALPHAD expressions of the coexisting phases. Only for ordering reactions can the CALPHAD free energy expression be adopted directly in the Landau polynomial used in the phase-field model, since in the CALPHAD approach the ordered and disordered phase are described with a single free energy expression that is coincidentally very similar to the Landau free energy density (18) used in the phase-field model for ordering reactions. This was illustrated by Zhu et al. [165] for quantitative simulations of the growth of ordered γ'-precipitates in Ni-based alloys.

Through extrapolation from lower-order systems, the CALPHAD approach allows us to obtain a full thermodynamic description of a multicomponent system using a limited amount of experimental information. From these thermodynamic descriptions, phase relationships and thermodynamic properties can be calculated for experimentally uninvestigated regions. The CALPHAD methodology is successful for determining bulk free energy expressions, since for most systems of technical interest there is a large amount of experimental data on thermodynamic properties and phase relationships available. In the case of the DICTRA mobility database, only a few systems have been optimized because the required experimental information is not available. Only a few laboratories are specialized in measuring diffusion coefficients, whereas the determination of phase equilibria and thermodynamic properties is much more common. Moreover, more mobility expressions must be optimized (a temperature-dependent and composition-dependent mobility expression must be determined for each component in each phase instead of a single expression for each phase for the Gibbs energy). Application of the CALPHAD approach for modeling the interfacial energy and mobility in multicomponent systems would be interesting, for example by optimizing temperature-dependent and composition-dependent expressions for the parameters in a model that describes the orientation dependence of the interfacial properties. However, it is even more difficult to measure interfacial energy and mobilities than to measure diffusion properties. Experimental information on interfacial properties is scarce, and relates mostly to pure materials.

7.1.2. Coupling with atomistic calculations

The phase-field simulation technique was also combined with ab initio calculations and other atomistic simulation techniques to obtain difficult-to-measure parameters. Vaithyanathan et al. [26,166,167] presented a multiscale approach based on ab initio calculations, mixed-cluster expansion Monte Carlo simulations and the phase-field method, for investigating the growth and coarsening of θ'-Al_2Cu precipitates during aging of an Al alloy. The free energy density, the interfacial energy and anisotropy, the stress-free lattice parameters and the elastic constants were determined based on ab initio calculations. Bishop and Carter [168] propose a coarse graining method for relating the atomic structure of a grain boundary obtained from atomistic simulations, with the evolution of a continuous order parameter across a diffuse interface in the phase-field model. Hoyt, Asta and Karma [169,170] determined from atomistic molecular dynamics simulations, the interfacial energy and mobility and their anisotropies for pure Ni, Au and Ag. The atomistic calculations were coupled with a phase-field model [171] to study quantitatively the dendritic growth in these metals as a function of the undercooling. They also computed the liquid diffusivities of pure Cu and Ni in the vicinity of their melting points [172].

In principle, all parameters in the phase-field model can be calculated using an atomistic technique. A multiscale approach that combines ab initio, other atomistic simulation techniques such as molecular dynamics, cluster expansion and atomistic Monte Carlo, and the mesoscale phase-field technique, would result in a quantitative and fully predictive simulation technique. However, at this moment, the quantitative results from atomistic simulations themselves are not very reliable. There may be large deviations, up to 200% or 300%, between values for the same properties calculated using different atomistic techniques or different approximations for the interaction potential. Moreover, most atomistic simulation techniques still require a number of model parameters that must be determined using experimental data.

7.2. Numerical solution of the phase-field equations

For the numerical solution of the phase-field equations, the continuous system is projected on a lattice of discrete points, as is illustrated in Fig. 12. The phase-field equations are also discretized, resulting in a set of algebraic equations. Solution of the algebraic equations yields the values of the phase-field variables in all lattice points. For the lattice depicted in Fig. 12, the set of algebraic equations contains $N_1 \times N_2$ equations and the same number of unknowns for each phase-field variable. The lattice spacing Δx must be fine enough to resolve the interfacial profile of the phase-field variables, i.e. there must be a few grid points within the interfacial region. At the same time, the dimensions of the system l_1 en l_2 must be large enough to cover the processes occurring on a larger scale. As a consequence, the numerical solution of the phase-field simulations for actual alloy systems involves an enormous number of lattice points, since $N_1 = l_1/\Delta x$ and $N_2 = l_2/\Delta x$. Since, at each time step, the value of the phase-field variables must be computed for all the grid points, phase-field simulations are quite computationally intensive. Moreover, a smaller lattice spacing involves a smaller time step in order to maintain numerical stability. Large computer memory is also required to treat the huge algebraic systems of equations with many unknowns.

A finite difference discretization technique using uniform lattice spacing, and with a central second-order stepping in space and forward stepping in time, is most widely used because of its simplicity. For the two-dimensional system in Fig. 12, discretization of the Ginzburg–Landau equation then

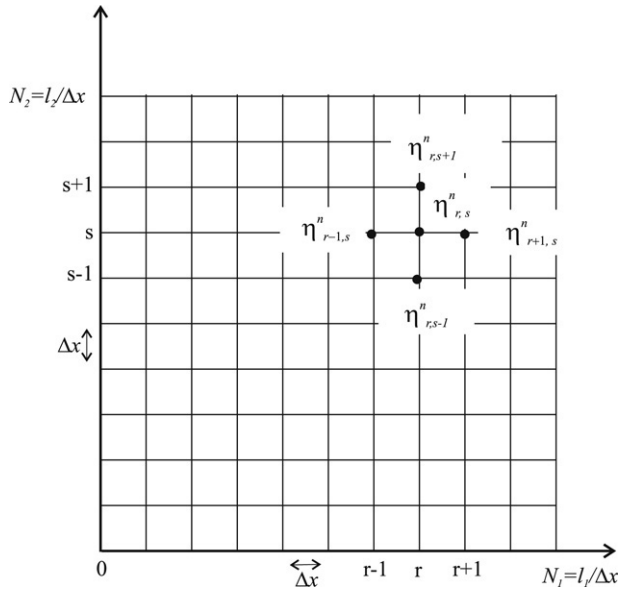

Fig. 12. Projection of a continuous phase-field variable on a lattice of discrete points for a two-dimensional system at time step n. Discretization of the partial differential phase-field equations results in a set of $N_1 \times N_2$ algebraic equations for each phase-field variable, that allows us to calculate, for each time step n, the values of the phase-field variables $\eta^n_{r,s}$ in all lattice points. l_1 and l_2 are the dimensions of the system, N_1 and N_2 the number of grid points in each dimension and Δx is the lattice spacing.

gives the following set of algebraic equations:

$$\frac{\eta^{n+1}_{r,s} - \eta^n_{r,s}}{\Delta t} = -L\left[\left(\frac{\partial f_0}{\partial \eta}\right)^n_{r,s} - \kappa \frac{\eta^n_{r-1,s} + \eta^n_{r,s-1} - 4\eta^n_{r,s} + \eta^n_{r+1,s} + \eta^n_{r,s+1}}{(\Delta x)^2}\right]. \quad (77)$$

The values of the phase-field variables at time step $n + 1$ are directly calculated from the values at time step n. The technique can be combined with Neumann, Dirichlet and periodic boundary conditions. However, it is well known that for such an explicit time stepping, the time step Δt must be very small to keep the numerical solution stable. The maximum time step is orders of magnitude smaller than the typical time span of microstructural evolution phenomena, resulting in long computation times. Sometimes a backward time stepping is applied to improve the stability conditions. The right-hand side in Eq. (77) is then evaluated on time step $n + 1$ instead of n, resulting in a system of coupled non-linear algebraic equations. The equations must be linearized, for example using a Newton–Raphson method, and iterative techniques, such as a conjugate gradient or multi-grid method, are required to solve the large system of equations. Thanks to the implicit time stepping, the time step can be taken larger; however, more numerical operations are required per time step and the implementation of the equations is more complicated than for the explicit time stepping. The gain in time highly depends on the application.

For solid-state phase transformations, the Fourier-spectral method with semi-implicit time stepping [173,174] is regularly applied. In this technique, the continuous phase-field equations are transformed into a set of algebraic equations in Fourier space by a discrete Fourier transformation. The resulting algebraic equations are solved, one by one, in Fourier space using a semi-implicit time stepping. The advantage of this method is that the gradient term can be treated implicitly without solving a large system of coupled algebraic equations. Spectral methods give a better spatial accuracy than the second-order finite difference discretization [173], and the semi-implicit time stepping allows a time step that is an order of magnitude larger than explicit time stepping. However, if the phase-field parameters depend on the phase-field variables, several Fourier transforms and back transforms must be performed for each time step, reducing the efficiency of the method. The Fourier-spectral method is only applicable for systems with periodic boundary conditions. Legendre- and Chebyshev-spectral methods enable other boundary conditions [175].

Finite volume or finite element discretizations based on an adaptive non-uniform grid have been developed for solidification simulations [57,56,91,176,177]. The non-uniform mesh has more grid points near the solid–liquid interface for a good resolution of the evolution of the phase-field across the interface. In the bulk domains, where the phase-field is constant, a coarser grid is applied to compute the evolution of the temperature and composition field. During the evolution of the structure, the mesh is adapted to the moving interface. The adaptive method allows us to consider heat and mass diffusion over much larger distances. Although the implementation of an adaptive-mesh technique is more complicated than that of a technique based on a uniform grid, the benefits may be considerable, certainly in the case of anisotropic interfacial properties where a fine resolution of the interface is required. For microstructures that consist of a large number of grains or precipitates, the classical adaptive meshing techniques are hard to apply. A spectral method combined with an adaptive moving mesh method [178] might be more appropriate for these structures.

Furthermore, algorithms and sparse data structures have been developed for polycrystalline structures represented by a large number of phase-field variables. For each phase-field variable, the corresponding evolution equation is only solved and its value is only stored for those grid points where its absolute value exceeds a small threshold value [104,179,180] or even only for the grid points at interfaces [181]. In this way, the calculation time and the required computer memory are significantly reduced. They scale only with the system size and are nearly independent of the number of phase-field variables involved in the simulation.

For three-dimensional simulations with realistic system size, parallel codes that distribute the calculation work and computer memory requirements over multiple computers are needed.

7.3. Nucleation

In many technical applications the microstructure of a material is tailored by controlling the nucleation and growth of a new forming phase at a particular step in the

production process. As microstructures are evolving non-equilibrium features, their current state is not only determined by the material properties and current process parameters, but also by previous microstructural processes. Therefore, in order to fully predict microstructure evolution, it is important to understand nucleation and include it correctly into microstructure simulations.

From a computational point of view, it is not feasible to consider nucleation and considerable growth at the same time in a phase-field simulation, since an extremely small spatial resolution and time step over the whole domain are required to catch the nucleation events. Therefore, most often, nucleation is incorporated ad hoc into the simulations [182, 52,183,159] using separate analytical models that describe the nucleation rate and the growth of critical nuclei as a function of the local conditions, such as the local temperature and composition. Once a nucleus has reached a size of the order of the grid spacing in the phase-field simulation, it is included as a new grain in the phase-field representation and its further growth is governed by the phase-field equations. This approach was, amongst others, applied to study the role of the cooling conditions on the evolution of the grain or particle size distribution for the growth of γ'-precipitates in Al–Ni alloys [182] and the equiaxed solidification in technical magnesium alloys [159]. The simulations help us to understand the effect of random nucleation on the evolution of a microstructure. However, the results can only be quantitative if the assumptions in the nucleation model are applicable for the material and process conditions concerned, and if the parameters in the model are known, which is mostly not the case. The approach cannot give any insight into the formation and properties of critical nuclei.

It was shown by Cahn and Hilliard [68] for spinodal decomposition and later by Gránásy et al. [156,157] for crystal growth in undercooled melts that the phase-field method, or in general diffuse-interface methods, are in fact very appropriate for studying nucleation and the initial stages of crystal growth. Different from the classical analytical models where nuclei are assumed to have homogeneous bulk properties (as for example the spherical cap model of Gibbs [184]), diffuse-interface models describe nuclei as local fluctuations or heterogeneities in properties like structure, density or composition. This latter approach is probably more realistic since nuclei may be so small that there is no homogeneous bulk material. The diffuse-interface description can also include in a straightforward way the effect of anisotropy and transport phenomena on the evolution of a nucleus or fluctuation. The properties of a critical fluctuation that can evolve spontaneously towards a mesoscale feature, and the nucleation barrier, are determined by the free energy functional in the phase-field model.

The diffuse-interface approach has been applied to study the properties and evolution of nuclei under various conditions (see [64,185] for an overview on phase-field simulations of crystal nucleation and growth). Phenomena like homogeneous nucleation, heterogeneous nucleation at walls and particles [186] and the effect of convection on the nucleation of a peritectic phase [187] were treated. The model was validated with experimental results for Ni–Cu melts [156, 157] and with molecular dynamics simulations for hard sphere systems [188]. Especially for systems far from thermodynamic equilibrium, for example in the case of strong undercooling or high supersaturation, the results obtained with phase-field simulations are very different from and more realistic than those obtained with the classical spherical cap model.

7.4. Diffuse-interface related issues and model validation

The diffuse-interface formulation has important advantages with respect to sharp-interface models, because no boundary conditions are specified at the interfaces between different domains. It enables us to study the evolution of arbitrary complex morphologies without any presumption on the shape of the grains and to predict non-equilibrium conditions at moving interfaces. It is also straightforward to account for the long-range elastic interactions that are involved in most solid-state transformations.

The drawback is that, due to the steep gradients in properties at the interfaces, simulations based on a diffuse-interface model can be extremely demanding from a computational point of view. Depending on the system and the temperature, the interfacial thickness in real materials ranges from a few angstroms to, at most, a few nanometers. As there must be at least 5–10 grid points within the interfacial regions to maintain numerical stability, only very small systems are feasible when using a uniform grid spacing, even with today's computer power. For two-dimensional simulations, the maximum system size is about 1 μm in each dimension; for three-dimensional simulations, it is of the order of only 100 nm. These dimensions are too small to study realistic microstructural phenomena which involve coarsening, long-range elastic interactions and diffusion processes. Therefore, in nearly all phase-field simulations, interfaces are taken artificially wide to increase the system size.

It is obvious that the artificial width of the interface is limited as well by the smallest features in the microstructure. Moreover, for many phase-field models, the profiles of the conserved and non-conserved field variables at interfaces are coupled in a complex way and there are not enough model parameters to modify the interfacial width for given interfacial energy and interface kinetics. Also the coalescence of neighboring particles and a number of non-equilibrium effects at interfaces, like solute trapping and solute drag, are exaggerated when interfaces are taken too wide. Consequently, increasing the interface width without concern seriously affects the simulation results. One of the current topics in phase-field modeling is the development of models that allow us to choose the interfaces artificially wide, without affecting the interface behavior. A number of strategies that were successful in suppressing part of the side-effects are discussed in the next paragraphs.

7.4.1. Controlling the interfacial profiles and interfacial energy

For arbitrary model formulations, the interfacial energy scales with the interfacial width, amongst other reasons because

there is a contribution to the interfacial energy from the concentration profiles [46]. Therefore, phase-field models have been developed with enough model parameters and particular choices for the interpolation function $p(\phi)$ and double- or multi-well function $g(\phi)$ in the free energy, so that it is possible to control the interfacial profiles of the phase-field variables.

The phenomenological single-phase-field models provide enough degrees of freedom to adjust for the artificial interfacial thickness l_{art}, as there are at least two parameters, namely κ and w, for defining the interfacial thickness and specific energy. When the restrictions (40) and (41) for the composition fields are imposed, the appropriate values for κ and w can be obtained easily. Combination of the relations (42) and (43) gives

$$\sigma_{\text{int}} = \frac{\alpha l_{\text{art}} w}{12}. \tag{78}$$

Hence, for an artificial interfacial width l_{art}, given by computational limitations, the height of the double-well potential w can be chosen to fit the actual interfacial energy. Once w is chosen, relation (43) with $l = l_{\text{art}}$ gives the appropriate value for κ.

For the multiphase-field models the interfacial width can be easily increased by adapting the values for κ_{jk} and m_{jk} in the free energy functional (51) or by taking a larger value for ϵ in the entropy functional (56). However, a problem of the multiphase-field formalism is that a third phase may appear at the interface between two phases, which affects the interfacial properties and complicates parameter assessment. Efforts are made to find formulations that reduce or avoid this unphysical third-phase effect. The numerical study of Garcke et al. [141], for example, shows that a multi-obstacle potential (58), in combination with higher-order terms $\propto \phi_i\phi_j\phi_k$, can diminish the interference of third phases at two-phase interfaces. The use of a double- or multi-obstacle potential also reduces to a certain extent the artificially large interaction between neighboring particles [101].

Phase-field models derived from Khachaturyan's microscopic theory, in most cases, do not have enough degrees of freedom to increase the interfacial thickness without changing the interfacial energy. One approach is to scale the time and spatial length and the energetic contributions to the thermodynamic free energy, based on a non-dimensionalized formulation of the phase-field model [165,189]. Another approach is to incorporate a multi-well function into the model, so that there is an extra degree of freedom for adjusting the interfacial width, and to change the formulation of the free energy functional so that the chemical free energy does not contribute to the interfacial energy. The classical model for ordered precipitates was, for example, reformulated in this way, in order to perform quantitative three-dimensional simulations for realistic length and time scales [130,190,191]. However, it is not yet clear how to treat coherency strains quantitatively correct when interfaces are artificially thick.

In the model of Echebarria et al. [53] and Folch and Plapp [192,54], the free energy is divided into an enthalpy and entropy contribution and the classical interpolation function $p(\phi)$ is replaced by two separate interpolation functions, one for the enthalpy and one for the entropy contribution. The interpolation functions relate to each other in such a way that for dilute alloys the concentration profile does not contribute to the interfacial energy. The interfacial thickness can accordingly be modified while the interfacial energy is kept constant, by changing the coefficients in front of the double-well potential and the gradient term. Different from the approaches above, in this model, there is no need to split up each concentration field in virtual concentration fields for each phase as in Eq. (42). Folch and Plapp also propose an alternative multi-well potential for systems with three phases that ensures the absence of a third phase at the interfaces. Although an extension of this multi-well potential towards systems with an arbitrary number of phases is in theory straightforward, it might result in impractical long equations.

In the model for grain growth in pure single-phase materials based on the order parameter representation [3,81,193], there are enough model parameters to choose the width of the grain boundaries independently from the grain boundary energies. Moreover, the model prevents in a natural way the presence of additional phases at grain boundaries. However, when the set of non-conserved order parameter fields is combined with a concentration field [89,90,88], it is no longer possible to increase the interfacial width without changing the interfacial energy. The amount of solute dissolved at interfaces also increases with interfacial thickness. There is no satisfying approach yet to circumvent these artificial effects.

7.4.2. *Corrections for kinetic and non-equilibrium effects*

As illustrated in Section 6.1 for curvature driven interface motion, it is common to relate the kinetic parameter in the Ginzburg–Landau or Cahn–Allen equations to measurable quantities by matching an asymptotic expansion of the phase-field model with the corresponding sharp-interface model, as sharp-interface models are usually formulated in terms of measurable quantities. The formulation and parameters of the phase-field model are preferentially chosen so that the corresponding sharp-interface model is recovered in the limit considered for the expansion. Sharp-interface asymptotic expansions [194,37,195,42,196], where the interface is assumed to have a zero thickness, and thin-interface asymptotic expansions [50,135,197], where the interface is assumed to have a finite thickness that is however much smaller than the smallest microstructural features, are most common. The sharp-interface expansion results in fixed (i.e. independent of the interface width) relations between the kinetic parameters in the phase-field model and those in the sharp-interface model, which are strictly spoken only valid for infinitely sharp interfaces. The thin-interface expansion gives expressions for the kinetic parameters that contain correction terms for the interfacial width. Numerous numerical tests have been performed to quantify the effect of the interface thickness on the results of a phase-field simulation and to test the validity of the asymptotic expansions.

For purely curvature driven interface movement, the kinetics are hardly affected by the width of the interface, as long as the interfacial profile is well resolved by the numerical grid and the

interfacial energy is correctly reproduced [198]. Only for grain sizes in the range of, and smaller than, the interfacial width, do the phase-field simulations deviate considerably from the sharp-interface kinetics. The sharp-interface asymptotics are thus well reproduced in the simulations, even when the interface is taken artificially wide.

However, when bulk driving forces and heat and mass diffusion are involved, the interface kinetics deviate considerably from the sharp-interface asymptotic behavior if the interface width is increased [135]. Especially when there is a large difference between the conductivities or diffusion coefficients on both sides of the interface, artificial non-equilibrium effects such as extra surface diffusion, interface stretching and solute trapping affect the numerical results [197,51]. Karma and Rappel [50,135] worked out a thin-interface asymptotic expansion of a phase-field model for the solidification of a pure material with equal conductivities in the liquid and the solid. They showed that the interface-thickness-dependent correction term for the kinetic parameter allows us to obtain quantitatively correct results for interface thicknesses that are several orders larger than is possible for a sharp-interface asymptotic expansion. A similar thin-interface analysis can be applied to alloy solidification [51,101,53,54]. To overcome the artificial effects caused by a difference in diffusion coefficient on both sides of the interface, the thin-interface matching was combined with a non-variational[9] anti-trapping current in the equation for mass conservation that counterbalances for the solute trapped at the artificially wide interfaces [51,53,54]. A similar correction term was also proposed by Shi et al. [199]. Up to now, the anti-trapping term has only been worked out for dilute solutions.

7.4.3. Quantitative validation with experimental data

Quantitative validation of the different phase-field models is frequently based on simulations for pure Ni and Ni–Cu alloys [156,56,176,91], since it is a simple system and its physical properties are quite well known. In the case of solid-state phase transformations, especially those involving elastic strains, analytical or sharp-interface models are less well established. Furthermore, materials showing a symmetry reducing or ordering transformation are, in general, complicated and difficult to characterize. Therefore, quantitative validation is more difficult for these models. The Ni–Al system is frequently used as a model system for quantitative simulations of ordering reactions [190,191], since, due to its technical relevance, the system is widely studied.

7.4.4. Phase-field crystal model

Very recently a new continuum modeling approach, the phase-field crystal model, was introduced [200–202]. It allows us to simulate microstructural behavior on atomistic length scales and diffusive time scales. Hence, the spatial resolution is of the same order as for molecular dynamics simulations; however, it is possible to consider much longer time scales. In the phase-field crystal model, the phase-field variable is the local atom density. For solid structures the free energy is minimal for periodic solutions of the density field, whereas in the liquid it is minimal for a constant value of the density field. Due to the periodicity of the density field and the atomic resolution, crystal anisotropy and the interaction between elastic lattice deformations, dislocation movement and plastic deformation [203] are incorporated automatically. Moreover, the diffuse-interface related problems of phase-field models are avoided. Up to now simulations have only been for two-dimensional systems and simple crystal structures. The possibilities of the technique are still to be explored further and efficient numerical techniques that exploit the periodicity of the solution have to be developed.

[9] Which means that the extra term cannot be derived from a free energy functional according to the principles of non-equilibrium thermodynamics.

8. Summary

This paper gives an introduction to the phase-field method and an overview of its possibilities. The phase-field method is a versatile and powerful technique for simulating microstructural evolution, which is currently very popular. Amongst others, it has been applied to solidification, precipitate growth and coarsening, martensitic transformations and grain growth and, more recently, also to other solid-state phase transformations like the austenite to ferrite transformation in steels, dislocation dynamics, crack propagation and nucleation. The achievements are increasing rapidly due to improved modeling and implementation techniques and growing computer capacities.

In the phase-field method, a microstructure is represented by means of a set of conserved and non-conserved phase-field variables that are continuous functions of spatial coordinates and time. The molar fraction fields of the constituting components are typical examples of a conserved phase-field variable. Non-conserved phase-field variables, such as order parameter fields and phase-fields, contain information on the local structure and orientation. Within domains the phase-field variables have nearly constant values, and at the interface they vary continuously over a narrow region between their values in the neighboring domains. Consequently, the interfaces have a finite width and the variations in properties at interfaces are continuous. This is called a diffuse-interface description. The main advantage of diffuse interfaces is that no boundary conditions must be specified at the moving interfaces. Therefore, phase-field models are able to predict complex morphological evolutions. Furthermore, no a priori assumptions on the (non-) equilibrium conditions at the moving interfaces are required.

Different from classical thermodynamics, the free energy in phase-field models is expressed as a functional of the phase-field variables and their spatial gradients. Since interfaces are characterized by a steep gradient in properties, the gradient term automatically gives rise to interfacial tension. For solid-state applications, the elastic strain energy due to transformation strains or an externally applied stress is formulated as a function of the phase-field variables using a continuum micro-elasticity approach.

A set of kinetic equations is solved numerically to obtain the temporal evolution of the phase-field variables. It is straightforward to include into a phase-field model the effect of different transport processes, such as diffusive mass and heat (conduction) transport, fluid flow and electric current, on the morphological evolution of the grains. Stochastic noise terms can be added to the equations to simulate nucleation or to induce instabilities in a metastable structure or steady-state growth morphology, although nucleation is usually incorporated into phase-field simulations using separate analytical nucleation models.

Phase-field models contain a large number of phenomenological parameters, which have to be determined in order to obtain quantitative results for real alloys. The parameters are related to the thermodynamic properties and equilibrium composition of the coexisting phases, the interfacial energy, width and mobility, the diffusion properties of the solute elements, and the elastic properties of all coexisting phases. Due to the large number of parameters and because some of them are related to properties that are difficult to measure, it is complicated to determine all the parameters in a phase-field model. Different methodologies have been proposed to make parameter assessment more efficient and to reduce the dependence on experimental measurements. Assessed databases, such as the Thermo-Calc and DICTRA databases developed using the CALPHAD approach, are, for example, useful for phase-field simulations for multicomponent alloys. Moreover, atomistic simulations can provide information on difficult-to-measure properties, such as the interfacial energy and mobility and their anisotropy. However, parameter assessment is still a major problem in phase-field modeling.

The numerical solution and implementation of phase-field equations is, in principle, relatively simple and straightforward, as there is no need to track the interfaces. However, the resolution of the numerical technique must be very fine to catch the steep transitions of the phase-field variables at interfaces. Simulations for realistic system sizes and time scales are therefore not feasible using the ordinary numerical techniques, because of excessive computation times and insufficient computer memory. A finite volume or finite element discretization using an adaptive mesh is often applied for simulating crystal growth in solidification. Then, the mesh is taken extremely fine at the solid–liquid interface, to resolve the transition of the phase-field variables, and coarse within the bulk domains, for describing the mass and heat transfer over macroscopic distances. For solid-state phase transformations, a Fourier-spectral method with semi-implicit time stepping and uniform mesh is usually more appropriate than a technique based on adaptive meshing because of the large number of grains or precipitates involved.

To increase the system size towards relevant dimensions, the width of the diffuse interface must be taken artificially large. Therefore, it is important to develop phase-field formulations that allow us to change the interface width without affecting the interfacial energy and mobility or introducing spurious effects. A lot of progress has been made in controlling the interfacial profiles of the phase-field variables and suppressing artificial kinetic and non-equilibrium effects, although a general solution has not yet been found and all strategies are still under debate.

Acknowledgements

This text is based on parts of the doctoral thesis of Nele Moelans (K.U. Leuven, May 2006, promotors Bart Blanpain and Patrick Wollants). The doctoral research was granted by the Institute for the Promotion of Innovation through Science and Technology in Flanders (IWT — Vlaanderen). From September 2006, Nele Moelans has been a Postdoctoral Fellow of the Research Foundation — Flanders (FWO — Vlaanderen). We thank both institutions for financial support. We also gratefully thank the other members of the examination commission, L. Froyen, P. Van Houtte, C. Creemers, B. Verlinden, S. Vandewalle and B. Nestler, for their interest, questions and comments.

References

[1] W.J. Boettinger, J.A. Warren, C. Beckermann, A. Karma, Phase-field simulation of solidification, Ann. Rev. Mater. Res. 23 (2002) 163–194.
[2] L.-Q. Chen, Phase-field models for microstructure evolution, Ann. Rev. Mater. Res. 32 (2002) 113–140.
[3] L.-Q. Chen, W. Yang, Computer simulation of the domain dynamics of quenched system with a large number of nonconserved order parameters: The grain-growth kinetics, Phys. Rev. B 50 (1994) 15752.
[4] S. Hu, L. Chen, Solute segregation and coherent nucleation and growth near a dislocation — A phase-field model integrating defect and phase microstructures, Acta Mater. 49 (2001) 463–472.
[5] D. Rodney, Y. LeBouar, F. A., Phase field methods and dislocations, Acta Mater. 51 (2003) 17–30.
[6] Y.U. Wang, Y.M. Jin, A.M. Cuitino, A.G. Khachaturyan, Phase field microelasticity theory and modeling of multiple dislocation dynamics, Appl. Phys. Lett. 78 (2001) 2324–2326.
[7] Y. Jin, Y. Wang, A. Khachaturyan, Three-dimensional phase field microelasticity theory and modelling of multiple cracks and voids, Appl. Phys. Lett. 29 (2001) 3071–3073.
[8] H. Henry, H. Levine, Dynamic instabilities of fracture under biaxial strain using a phase field model, Phys. Rev. Lett. 93 (2004) 105504.
[9] D. Bhate, A. Kumar, A. Bower, Diffuse interface model for electromigration and stress voiding, J. Appl. Phys. 87 (2000) 1712–1721.
[10] A. Kazaryan, Y. Wang, B. Patton, Generalized phase field approach for computer simulation of sintering: Incorporation of rigid-body motion, Scripta Mater. 41 (1999) 487–492.
[11] X. Jing, J. Zhao, G. Subhash, X.-L. Gao, Anisotropic grain growth with pore drag under applied loads, Mater. Sci. Eng. A 412 (2005) 271–278.
[12] Y. Wang, Computer modeling and simulation of solid-state sintering: A phase field approach, Acta Mater. 54 (2006) 953–961.
[13] Q. Du, C. Liu, X. Wang, Simulating the deformation of vesicle membranes under elastic bending energy in three dimensions, J. Comput. Phys. 212 (2006) 757–777.
[14] T. Biben, K. Kassner, C. Misbah, Phase-field approach to three-dimensional vesicle dynamics, Phys. Rev. E 72 (2005) 041921.
[15] J. Rowlinson, Translation of J.D. van der Waals' "The thermodynamic theory of capillarity under the hypothesis of a continuous variation of density", J. Statist. Phys. 20 (2) (1979) 197–245.
[16] V. Ginzburg, L. Landau, On the theory of superconductivity, Zh. Eksp. Teor. Fiz. 20 (1950) 1064–1082. Translation in Collected papers of L.D. Landau, Pergamon, Oxford, 1965, pp. 546–568.
[17] J.W. Cahn, J.E. Hilliard, Free energy of a nonuniform system. I. Interfacial free energy, J. Chem. Phys. 28 (1958) 258–267.
[18] P. Hohenberg, B. Halperin, Theory of dynamic critical phenomena, Rev. Modern Phys. 49 (1977) 435–479.

[19] J. Gunton, M. Miguel, P. Sahni, in: C. Domb, J.L. Lebowitz (Eds.), The Dynamics of First-Order Phase Transitions, vol. 8, Academic press, New York, 1983, pp. 267–466. Ch. 3.
[20] L.-Q. Chen, A. Khachaturyan, Computer simulation of structural transformations during precipitation of an ordered intermetallic phase, Acta Mater. 39 (1991) 2533–2551.
[21] Y. Wang, L.-Q. Chen, A.G. Khachaturyan, Kinetics of strain-induced morphological transformation in cubic alloys with a miscibility gap, Acta Metall. Mater. 41 (1) (1993) 279–296.
[22] A. Khachaturyan, Microscopic theory of diffusion in crystalline solid solutions and the time evolution of the diffuse scattering of X rays and thermal neutrons, Sov. Phys. Solid State 9 (1968) 2040–2046. Engl. Transl. of Fiz. Tverd. Tela.
[23] A.-G. Khachaturyan, Theory of Structural Transformations in Solids, Wiley-Interscience publications, Wiley, New York, 1983.
[24] Y. Wang, D. Banerjee, C. Su, A. Khachaturyan, Field kinetic model and computer simulation of precipitation of $L1_2$ ordered intermetallics from f.c.c. solid solution, Acta Mater. 46 (1998) 2983–3001.
[25] D. Li, L. Chen, Shape evolution and splitting of coherent particles under applied stresses, Acta Mater. 47 (1999) 247–257.
[26] V. Vaithyanathan, Phase-field simulations of coherent precipitate morphologies and coarsening kinetics, Ph.D. Thesis, The Pennsylvania State University, Department of Materials Science and Engineering, May 2002.
[27] Y. Wang, A. Khachaturyan, Three-dimensional field model and computer modeling of martensitic transformations, Acta Mater. 45 (1997) 759–773.
[28] A. Artemev, Y. Jin, A. Khachaturyan, Three-dimensional phase field model of proper martensitic transformation, Acta Mater. 49 (2001) 1165–1177.
[29] Y. Li, S. Hu, Z. Liu, L. Chen, Phase-field model of domain structures in ferroelectric thin films, Appl. Phys. Lett. 78 (2001) 3878–3880.
[30] S. Choudhury, Y. Li, C. Kril III, L.-Q. Chen, Phase-field simulation of polarization switching and domain evolution in ferroelectric polycrystals, Acta Mater. 53 (2005) 5313–5321.
[31] J. Zhang, L. Chen, Phase-field microelasticity theory and micromagnetic simulations of domain structures in giant magnetostrictive materials, Acta Mater. 53 (2005) 2845–2855.
[32] T. Miyazaki, A. Takeuchi, T. Koyama, T. Kozakai, Computer simulation of phase decomposition in the regular solid solution based upon the Cahn–Hilliard's non-linear diffusion equation, Mater. Trans. JIM 32 (1991) 915–920.
[33] T. Miyazaki, A. Takeuchi, T. Koyama, Computer simulations of the phase decomposition on Cu–Co binary alloys based on the non-linear diffusion equation, J. Mater. Sci. 27 (1992) 2444–2448.
[34] H. Nishimori, A. Onuki, Pattern formation in phase-separating alloys with cubic symmetry, Phys. Rev. B 42 (1990) 980–983.
[35] Y. Le Bouar, A. Loiseau, A. Khachaturyan, Origin of chessboard-like structures in decomposing alloys, theoretical model and computer simulation, Acta Mater. 46 (1998) 2777–2788.
[36] A. Finel, G. Boussinot, Y. Le Bouar, Q. Bronchart, Quantitative phase field modeling, JOM 56 (2004) 215.
[37] J. Langer, Models of pattern formation in first-order phase transitions, in: G. Grinstein, G. Mazenko (Eds.), Directions in Condensed Matter Physics, World scientific, Singapore, 1986, pp. 165–185.
[38] M. Ode, S. Kim, T. Suzuki, Recent advances in the phase-field model for solidification, ISIJ Int. 41 (2001) 1076–1082.
[39] G. Caginalp, P. Fife, Phase-field methods for interfacial boundaries, Phys. Rev. B 33 (11) (1986) 7792–7794.
[40] G. Caginalp, P. Fife, Higher-order phase field models and detailed anisotropy, Phys. Rev. B 34 (1986) 4940–4943.
[41] O. Penrose, P. Fife, Thermodynamically consistent models of phase-field type for the kinetics of phase transitions, Physica D 43 (1990) 44–62.
[42] S.-L. Wang, R.F. Sekerka, A.A. Wheeler, B.T. Murray, S.R. Coriell, R.J. Braun, G.B. McFadden, Thermodynamically-consistent phase-field models for solidification, Physica D 69 (1993) 189–200.
[43] R. Kobayashi, Modeling and numerical simulations of dendritic crystal growth, Physica D 63 (1993) 410–423.
[44] A.A. Wheeler, W.J. Boettinger, G.B. McFadden, Phase-field model for isothermal phase transitions in binary alloys, Phys. Rev. A 45 (1992) 7424–7439.
[45] G. McFadden, A. Wheeler, R. Braun, S. Coriell, R. Sekerka, Phase-field models for anisotropic interfaces, Phys. Rev. E 48 (1993) 2016–2024.
[46] A. Wheeler, W. Boettinger, G. McFadden, Phase-field model of solute trapping during solidification, Phys. Rev. E 47 (1993) 1893–1909.
[47] A. Wheeler, G. McFadden, W. Boettinger, Phase-field model for solidification of a eutectic alloy, Proc. R. Soc. Lond. A 452 (1996) 495–525.
[48] A. Wheeler, G. McFadden, A ξ-vector formulation of anisotropic phase-field models: 3D asymptotics, Euro. J. Appl. Math. 7 (1996) 367–381.
[49] S. Kim, W. Kim, T. Suzuki, Phase-field model for binary alloys, Phys. Rev. E 60 (1999) 7186–7196.
[50] A. Karma, W.-J. Rappel, Phase-field method for computationally efficient modeling of solidification with arbitrary interface kinetics, Phys. Rev. E 53 (1996) R3017–R3020.
[51] A. Karma, Phase-field formulation for quantitative modeling of alloy solidification, Phys. Rev. Lett. 87 (2001) 115701.
[52] T.S. Lo, A. Karma, M. Plapp, Phase-field modeling of microstructural pattern formation during directional solidification of peritectic alloys without morphological instability, Phys. Rev. E 63 (2001) 031504.
[53] B. Echebarria, R. Folch, A. Karma, M. Plapp, Quantitative phase-field model of alloy solidification, Phys. Rev. E 70 (2004) 061604.
[54] R. Folch, M. Plapp, Quantitative phase-field modeling of two-phase growth, Phys. Rev. E 72 (2005) 011602.
[55] C. Andersson, Phase-field simulation of dendritic solidification, Ph.D. Thesis, Royal Institute of Technology, 2002.
[56] I. Loginova, J. Odqvist, G. Amberg, J. Ågren, The phase-field approach and solute drag modeling of the transition to massive $\gamma \rightarrow \alpha$ transformation in binary Fe–C alloys, Acta Mater. 51 (2003) 1327–1339.
[57] R. Tonhardt, G. Amberg, Phase-field simulation of dendritic growth in a shear flow, J. Cryst. Growth 194 (1998) 406–425.
[58] I. Steinbach, F. Pezzolla, B. Nestler, M. Seeßelber, R. Prieler, G.J. Schmitz, J.L.L. Rezende, A phase field concept for multiphase systems, Physica D 94 (1996) 135–147.
[59] J. Tiaden, B. Nestler, H. Diepers, I. Steinbach, The multiphase-field model with an integrated concept for modelling solute diffusion, Physica D 115 (1998) 73–86.
[60] H. Garcke, B. Nestler, B. Stinner, A diffuse interface model for alloys with multiple components and phases, SIAM J. Appl. Math. 64 (2004) 775–799.
[61] B. Nestler, H. Garcke, B. Stinner, Multicomponent alloy solidification: Phase field modeling and simulations, Phys. Rev. E 71 (2005) 041609.
[62] R. Kobayashi, J.A. Warren, W.C. Carter, Vector-valued phase field model for crystallization and grain boundary formation, Physica D 119 (1998) 415–423.
[63] H. Kobayashi, M. Ode, S. Kim, W. Kim, T. Suzuki, Phase-field model for solidification of ternary alloys coupled with thermodynamic database, Scr. Mater. 48 (2003) 689–694.
[64] L. Gránásy, T. Pusztai, T. Börzsönyi, G. Tóth, G. Tegze, Phase field theory of crystal nucleation and polycrystalline growth: A review, J. Mater. Res. 21 (2006) 309–319.
[65] A. Onuki, Ginzburg–Landau approach to elastic effects in the phase separation of solids, J. Phys. Soc. Jpn. 58 (1989) 3065–3068.
[66] J. Zhu, L.-Q. Chen, J. Shen, Morphological evolution during phase separation and coarsening with strong inhomogeneous elasticity, Model. Simul. Mater. Sci. Eng. 9 (2001) 499–511.
[67] D. Orlikowski, C. Sagui, A. Somoza, C. Roland, Large-scale simulations of phase separation of elastically coherent binary alloy systems, Phys. Rev. B 59 (1999) 8646–8659.
[68] J. Cahn, J. Hilliard, Free energy of a nonuniform system. III: Nucleation in a two-component incompressible fluid, J. Chem. Phys. 31 (3) (1959) 688–699.
[69] S. Hu, L. Chen, A phase-field model for evolving microstructures with strong elastic inhomogeneity, Acta Mater. 49 (2001) 1879–1890.
[70] K. Wu, J. Morral, Y. Wang, A phase field study of microstructural changes due to the Kirkendall effect in two-phase diffusion couples, Acta Mater. 49 (2001) 3401–3408.

[71] W. Dreyer, W. Müller, A study of the coarsening in tin/lead solders, Int. J. Solids Struct. 37 (2000) 3841–3871.
[72] W. Dreyer, W. Müller, Modeling diffusional coarsening in eutectic tin/lead solders: A quantitative approach, Int. J. Solids Struct. 38 (2001) 1433–1458.
[73] J.-C. Tolédano, P. Tolédano, The Landau theory of phase transitions. Application to structural, incommensurate, magnetic, and liquid crystal systems, in: World Scientific Lecture Notes in Physics, vol. 3, World Scientific Publishing Co. Pte. Ltd., 1987.
[74] S.M. Allen, J.W. Cahn, A microscopic theory for antiphase boundary motion and its application to antiphase domain coarsening, Acta Metall. 27 (1979) 1085–1095.
[75] Y. Wang, A. Khachaturyan, Effect of antiphase domains on shape and spatial arrangement of coherent ordered intermetallics, Scr. Metall. Mater. 31 (1994) 1425–1430.
[76] V. Vaithyanathan, L. Chen, Coarsening of ordered intermetallic precipitates with coherency stress, Acta Mater. 50 (2002) 4061–4073.
[77] D. Li, L. Chen, Shape of a rhombohedral coherent $Ti_{11}Ni_{14}$ precipitate in a cubic matrix and its growth and dissolution during constrained aging, Acta Mater. 45 (1997) 2435–2442.
[78] Y. Wen, Y. Wang, L. Chen, Effect of elastic interaction on the formation of a complex multi-domain microstructural pattern during a coherent hexagonal to orthorhombic transformation, Acta Mater. 47 (1999) 4375–4386.
[79] Y. Wen, Y. Wang, L. Chen, Coarsening dynamics of self-accommodating coherent patterns, Acta Mater. 50 (2002) 13–21.
[80] L.-Q. Chen, A novel computer simulation technique for modeling grain growth, Scr. Metall. Mater. 32 (1995) 115.
[81] D. Fan, L.-Q. Chen, Computer simulation of grain growth using a continuum field model, Acta Mater. 45 (1997) 611–622.
[82] D. Fan, C. Geng, L.-Q. Chen, Computer simulation of topological evolution in 2-D grain growth using a continuum diffuse-interface field model, Acta Mater. 45 (1997) 1115–1126.
[83] C.E. Krill, L.-Q. Chen, Computer simulation of 3-D grain growth using a phase-field model, Acta Mater. 50 (2002) 3057–3073.
[84] A. Kazaryan, Y. Wang, S.A. Dregia, B.R. Patton, Grain growth in anisotropic systems: Comparison of effects of energy and mobility, Acta Mater. 50 (2002) 2491–2502.
[85] Y. Suwa, Y. Saito, Computer simulation of grain growth by the phase field model. Effect of interfacial energy on kinetics of grain growth, Mater. Trans. 44 (11) (2003) 2245–2251.
[86] N. Ma, A. Kazaryan, S.A. Dregia, Y. Wang, Computer simulation of texture evolution during grain growth: Effect of boundary properties and initial microstructure, Acta Mater. 52 (2004) 3869–3879.
[87] N. Moelans, B. Blanpain, P. Wollants, Pinning effect of second-phase particles on grain growth in polycrystalline films studied by 3-d phase field simulations, Acta Mater. 55 (2007) 2173–2182.
[88] D. Fan, S.P. Chen, L.-Q. Chen, Computer simulation of grain growth kinetics with solute drag, J. Mater. Res. 14 (1999) 1113–1123.
[89] D. Fan, L.-Q. Chen, Diffusion-controlled grain growth in two-phase solids, Acta Mater. 45 (1997) 3297–3310.
[90] D. Fan, L.-Q. Chen, S.-P.P. Chen, Numerical simulation of zener pinning with growing second-phase particles, J. Am. Ceram. Soc. 81 (1998) 526–532.
[91] C. Lan, Y. Chang, C. Shih, Adaptive phase field simulation of non-isothermal free dendritic growth of a binary alloy, Acta Mater. 51 (2003) 1857–1869.
[92] J. Ramirez, C. Beckermann, Examination of binary alloy free dendritic growth theories with a phase-field model, Acta Mater. 53 (2005) 1721–1736.
[93] B. Nestler, D. Danilov, P. Galenko, Crystal growth of pure substances: Phase-field simulations in comparison with analytical and experimental results, J. Comput. Phys. 207 (2005) 221–239.
[94] C. Lan, Y. Chang, Efficient adaptive phase field simulation of directional solidification of a binary alloy, J. Cryst. Growth 250 (2003) 525–537.
[95] F. Drolet, K. Elder, M. Grant, J. Kosterlitz, Phase-field modeling of eutectic growth, Phys. Rev. E 61 (2000) 6705–6720.
[96] J. Warren, W. Boettinger, Prediction of dendritic growth and microsegregation patterns in a binary alloy using the phase-field method, Acta Metall. Mater. 43 (1995) 689–703.
[97] N. Ahmad, A. Wheeler, W. Boettinger, G. McFadden, Solute trapping and solute drag in a phase-field model of rapid solidification, Phys. Rev. E 58 (1998) 3436–3450.
[98] I. Loginova, J. Ågren, G. Amberg, On the formation of Widmanstätten ferrite in binary Fe–C — phase-field approach, Acta Mater. 52 (2004) 4055–4063.
[99] M. Mecozzi, J. Sietsma, S. van der Zwaag, Phase field modelling of the interfacial condition at the moving interphase during the $\gamma \rightarrow \alpha$ transformation in C–Mn steels, Comput. Mater. Sci. 34 (2005) 290–297.
[100] B. Nestler, A. Wheeler, Phase-field modeling of multi-phase solidification, Comput. Phys. Commun. 147 (2002) 230–233.
[101] S. Kim, W. Kim, T. Suzuki, M. Ode, Phase-field modeling of eutectic solidification, J. Cryst. Growth 261 (2004) 135–158.
[102] M. Apel, B. Boettger, H.-J. Diepers, I. Steinbach, 2D and 3D phase-field simulations of lamella and fibrous eutectic growth, J. Cryst. Growth 237–239 (2002) 154–158.
[103] M. Plapp, A. Karma, Eutectic colony formation: A phase-field study, Phys. Rev. E 66 (2002) 061608.
[104] S. Kim, D. Kim, W. Kim, Y. Park, Computer simulations of 2d and 3d ideal grain growth, Phys. Rev. E 74 (2006) 061605.
[105] K. Nakajima, I. Apel, I. Steinbach, The role of carbon diffusion in ferrite on the kinetics of cooperative growth of pearlite: A multi-phase field study, Acta Mater. 54 (2006) 3665–3672.
[106] I. Steinbach, A. Apel, The influence of lattice strain on pearlite formation in Fe-c, Acta Mater. 55 (2007) 4817–4822.
[107] D. Kondepudi, I. Prigogine, Modern Thermodynamics. From Heat Engines to Dissipative Structures, John Wiley & Sons Ltd, 1998.
[108] G. Rubin, A. Khachaturyan, Three-dimensional model of precipitation of ordered intermetallics, Acta Mater. 47 (1999) 1995–2002.
[109] R. Braun, J. Cahn, G. McFadden, A. Wheeler, Anisotropy of interfaces in an ordered alloy: A multiple-order-parameter model, Phil. Trans. R. Soc. Lond. A 355 (1997) 1787–1833.
[110] T. Abinandanan, F. Haider, An extended Cahn–Hilliard model for interfaces with cubic anisotropy, Phil. Mag. A 81 (2001) 2457–2579.
[111] P. Fratzl, O. Penrose, Modeling of phase separation in alloys with coherent elastic misfit, J. Statist. Phys. 95 (1999) 1429–1503.
[112] L. Chen, S. Hu, Phase field method applied to strain-dominated microstructure evolution during solid-state phase transformations, in: D. Raabe, F. Roters, F. Barlat, L.Q. Chen (Eds.), Continuum Scale Simulation of Engineering Materials: Fundamentals – Microstructures – Process Applications, Wiley-VCH Verlag GmbH & Co. KGa A, Weinheim, 2004, pp. 271–292.
[113] A. Khachaturyan, G.A. Shatalov, Theory of macroscopic periodicity for a phase transition in the solid state, Sov. Phys. JETP 29 (1969) 557–561. Engl. Trans. of Zk. Eksp. Teor. Fiz.
[114] A.G. Khachaturyan, Some questions concerning the theory of phase transformations in solids, Sov. Phys. Solid State 8 (1967) 2163–2168. Engl. Transl. of Fiz. Tverd. Tela.
[115] Y.U. Wang, Y.M. Jin, A.G. Khachaturyan, Phase field microelasticity theory and modeling of elastically and structurally inhomogeneous solid, J. Appl. Phys. 92 (2002) 1351–1360.
[116] P. Yu, S. Hu, L. Chen, Q. Du, An iterative-perturbation scheme for treating inhomogeneous elasticity in phase-field models, J. Comput. Phys. 208 (2005) 34–50.
[117] D. Seol, S. Hu, Y. Li, J. Shen, K. Oh, L. Chen, Computer simulation of spinodal decomposition in constrained films, Acta Mater. 51 (2003) 5173–5185.
[118] P. Leo, J. Lowengrub, H. Jou, A diffuse interface model for microstructural evolution in elastically stressed solids, Acta Mater. 46 (1998) 2113–2130.
[119] A. Artemev, Y. Jin, A. Khachaturyan, Three-dimensional phase field model and simulation of cubic → tetragonal martensitic transformation in polycrystals, Phil. Mag. A 82 (2002) 1249–1270.

[120] Y. Jin, A. Artemev, A. Khachaturyan, Three-dimensional phase field model of low-symmetry martensitic transformation in polycrystal: Simulation of ζ_2' martensitic in AuCd alloys, Acta Mater. 49 (2001) 2309–2320.
[121] Y. Wang, Y. Jin, A. Khachaturyan, The effect of free surfaces on martensite microstructures: 3D phase field microelasticity simulation study, Acta Mater. 52 (2004) 1039–1050.
[122] S. Hu, L. Chen, Diffuse-interface modeling of composition evolution in the presence of structural defects, Comput. Mater. Sci. 23 (2002) 270–282.
[123] Y. Wang, Y. Jin, A. Cuitino, A. Khachaturyan, Nanoscale phase field microelasticity theory of dislocations: Model and 3D simulations, Acta Mater. 49 (2001) 1847–1857.
[124] C. Shen, Y. Wang, Phase field model of dislocation networks, Acta Mater. 51 (2003) 2595–2610.
[125] H.-L. Hu, L.-Q. Chen, Three-dimensional computer simulation of ferroelectric domain formation, J. Am. Ceram. Soc. 81 (1998) 492–500.
[126] X. Guo, S.-Q. Shi, X. Ma, Elastoplastic phase field model for microstructure evolution, Appl. Phys. Lett. 87 (2005) 221910.
[127] S. Hu, M. Baskes, M. Stan, Phase-field modeling of microvoid evolution under elastic–plastic deformation, Appl. Phys. Lett. 90 (2007) 081921.
[128] J.-M. Debierre, A. Karma, F. Celestini, R. Guérin, Phase-field approach for faceted solidification, Phys. Rev. E 68 (2003) 041604.
[129] I. Loginova, Phase-field modeling of diffusion controlled phase transformations, Ph.D. Thesis, Royal Institute of Technology, Department of Mechanics, 2003.
[130] S. Hu, Phase-field models of microstructure evolution in a system with elastic inhomogeneity and defects, Ph.D. Thesis, The Pennsylvania State University, Department of Materials Science and Engineering, 2004.
[131] J. Taylor, J. Cahn, Diffuse interfaces with sharp corners and facets: Phase field models with strongly anisotropic surfaces, Physica D 112 (1998) 381–411.
[132] J. Eggleston, G. McFadden, P. Voorhees, A phase-field model for highly anisotropic interfacial energy, Physica D 150 (2001) 91–103.
[133] T. Uehara, R. Sekerka, Phase field simulations of faceted growth for strong anisotropy of kinetic coefficient, J. Cryst. Growth 254 (2003) 251–261.
[134] A. Karma, W.-J. Rappel, Numerical simulation of three-dimensional dendritic growth, Phys. Rev. Lett. 77 (1996) 4050–4053.
[135] A. Karma, W.-J. Rappel, Quantitative phase-field modeling of dendritic growth in two and three dimensions, Phys. Rev. E 57 (1998) 4323–4349.
[136] N. Ma, Q. Chen, Y. Wang, Implementation of high interfacial energy anisotropy in phase field simulations, Scripta Mater. 54 (2006) 1919–1924.
[137] H. Alt, I. Pawlow, A mathematical model of dynamics of non-isothermal phase separation, Physica D 59 (1992) 389–416.
[138] I. Loginova, G. Amberg, J. Ägren, Phase-field simulations of non-isothermal binary alloy solidification, Acta Mater. 49 (2001) 573–581.
[139] J. Eiken, B. Böttger, I. Steinbach, Multiphase-field approach for multicomponent alloys with extrapolation scheme for numerical application, Phys. Rev. E 73 (2006) 066122.
[140] B. Nestler, A. Wheeler, Anisotropic multi-phase-field model: Interfaces and junctions, Phys. Rev. E 57 (1998) 2602–2609.
[141] H. Garcke, B. Nestler, B. Stoth, A multiphase field concept: Numerical simulations of moving phase boundaries and multiple junctions, SIAM J. Appl. Math. 60 (1999) 295–315.
[142] B. Nestler, Motion of multiple interfaces: Grain growth and coarsening, in: D. Raabe, F. Roters, F. Barbat, L.-Q. Chen (Eds.), Continuum Scale Simulation of Engineering Materials, Wiley-VCH Verlag GmbH & Co. KGa A, Weinheim, 2004, pp. 327–342.
[143] I. Steinbach, M. Apel, Multi phase field model for solid state transformation with elastic strain, Physica D 217 (2006) 153–160.
[144] R. Spatschek, C. Muller-Gugenberger, E. Brener, B. Nestler, Phase field modeling of fracture and stress-induced phase transitions, Phys. Rev. E 75 (2007) 066111.
[145] S. De Groot, P. Mazur, Non-Equilibrium Thermodynamics, 1st edition, North-Holland Publishing Company, Amsterdam, 1963.
[146] M. Furtkamp, G. Gottstein, D.A. Molodov, V.N. Semenov, L.S. Shvindlerman, Grain boundary migration in Fe–3.5% Si bicrystals with [001] tilt boundaries, Acta Metall. 46 (1998) 4103–4110.
[147] J.-O. Andersson, J. Ågren, Models for numerical treatment of multicomponent diffusion in simple phases, J. Appl. Phys. 72 (1992) 1350–1355.
[148] B. Nestler, A. Wheeler, L. Ratke, C. Stöcker, Phase-field model for solidification of a monotectic alloy with convection, Physica D 141 (2000) 133–154.
[149] R. Tonhardt, G. Amberg, Dendritic growth of randomly oriented nuclei in a shear flow, J. Cryst. Growth 213 (2000) 161–187.
[150] C. Beckermann, H. Diepers, I. Steinbach, A. Karma, X. Tonga, Modeling melt convection in phase-field simulations of solidification, J. Comput. Phys. 154 (1999) 468–496.
[151] H. Diepers, C. Beckermann, I. Steinbach, Simulation of convection and ripening in a binary alloy mush using the phase-field method, Acta Mater. 47 (1999) 3663–3678.
[152] D. Anderson, G. McFadden, A. Wheeler, A phase-field model of solidification with convection, Physica D 135 (2000) 175–194.
[153] W. Miller, I. Rasin, F. Pimentel, Growth kinetics and melt convection, J. Cryst. Growth 266 (2004) 283–288.
[154] L. Brush, A phase field model with electric current, J. Cryst. Growth 247 (2003) 587–596.
[155] A. Karma, W.-J. Rappel, Phase-field model of dendritic sidebranching with thermal noise, Phys. Rev. E 60 (1999) 3614–3625.
[156] L. Gránásy, T. Börzsönyi, T. Pusztai, Nucleation and bulk crystallization in binary phase field theory, Phys. Rev. Lett. 88 (2002) 206105.
[157] L. Gránásy, T. Börzsönyi, T. Pusztai, Crystal nucleation and growth in binary phase-field theory, J. Cryst. Growth 237–239 (2002) 1813–1817.
[158] A. Engström, L. Höglund, J. Ågren, Computer simulation of diffusion in multiphase systems, Metall. Mater. Trans. A 25 (1994) 1127–1134.
[159] B. Böttger, J. Eiken, I. Steinbach, Phase field simulation of equiaxed solidification in technical alloys, Acta Mater. 54 (2006) 2697–2704.
[160] K. Wu, Y. Chang, Y. Wang, simulating interdiffusion microstructures in Ni–Al–Cr diffusion couples: A phase field approach coupled with CALPHAD database, Scr. Mater. 50 (2004) 1145–1150.
[161] U. Grafe, B. Böttger, J. Tiaden, S. Fries, Coupling of multicomponent thermodynamic databases to a phase field model: Application to solidification and solid state transformations of superalloys, Scr. Mater. 42 (2000) 1179–1186.
[162] Q. Chen, N. Ma, K. Wu, Y. Wang, Quantitative phase field modeling of diffusion-controlled precipitate growth and dissolution in Ti–Al–V, Scr. Mater. 50 (2004) 471–476.
[163] J. Huh, K. Hong, Y. Kim, K. Kim, Phase-field simulations of intermetallic compound growth during soldering reactions, J. Electron. Mater. 33 (2004) 1161–1170.
[164] A. Umantsev, Modeling of intermediate phase growth, J. Appl. Phys. 101 (2007) 024910.
[165] J. Zhu, Z. Liu, V. Vaithyanathan, L. Chen, Linking phase-field model to CALPHAD: Application to precipitate shape evolution in Ni-base alloys, Scr. Mater. 46 (2002) 401–406.
[166] V. Vaithyanathan, C. Wolverton, L.Q. Chen, Multiscale modeling of precipitate microstructure evolution, Phys. Rev. Lett. 88 (2002) 125503.
[167] V. Vaithyanathan, C. Wolverton, L.Q. Chen, Multiscale modeling of θ' precipitation in Al–Cu binary alloys, Acta Mater. 52 (2004) 2973–2987.
[168] C. Bishop, W. Carter, Relating atomistic grain boundary simulation results to the phase-field model, Comput. Mater. Sci. 25 (2002) 378–386.
[169] J. Hoyt, M. Asta, Atomistic computation of liquid diffusivity, solid–liquid interfacial free energy, and kinetic coefficient in Au and Ag, Phys. Rev. B 65 (2002) 214106.
[170] J. Hoyt, M. Asta, A. Karma, Atomistic and continuum modeling of dendritic solidification, Mater. Sci. Eng. R-Rep. 41 (2003) 121–163.
[171] J. Bragard, A. Karma, Y. Lee, M. Plapp, Linking phase-field and atomistic simulations to model dendritic solidification in highly undercooled melts, Interface Sci. 10 (2002) 121–136.
[172] J. Hoyt, B. Sadigh, M. Asta, S. Foils, Kinetic phase field parameters for the Cu–Ni system derived from atomistic computations, Acta Mater. 47 (1999) 3181–3187.

[173] L.-Q. Chen, J. Shen, Application of semi-implicit fourier-spectral method to phase field equations, Comp. Phys. Comm. 108 (1998) 147–158.
[174] J. Zhu, L.-Q. Chen, J. Shen, V. Tikare, Coarsening kinetics from a variable-mobility Cahn–Hilliard equation: Application of a semi-implicit fourier spectral method, Phys. Rev. E 60 (1999) 3564–3572.
[175] J. Zhu, L.-Q. Chen, J. Shen, V. Tikare, Microstructure dependence of diffusional transport, Comput. Mater. Sci. 20 (2001) 37–47.
[176] D. Danilov, B. Nestler, Dendritic to globular morphology transition in ternary alloy solidification, Phys. Rev. Lett. 93 (2004) 215501.
[177] D. Danilov, B. Nestler, Phase-field simulations of solidification in binary and ternary systems using a finite element method, J. Cryst. Growth 275 (2005) e177–e182.
[178] W. Feng, P. Yu, S. Hu, Z. Liu, Q. Du, L. Chen, Spectral implementation of an adaptive moving mesh method for phase-field equations, J. Comput. Phys. 220 (2006) 498–510.
[179] J. Gruber, N. Ma, Y. Wang, A. Rollett, G. Rohrer, Sparse data structure and algorithm for the phase field method, Modelling Simul. Mater. Sci. Eng. 14 (2006) 1189–1195.
[180] L. Vanherpe, N. Moelans, S. Vandewalle, B. Blanpain, Bounding box algorithm for three-dimensional phase field simulations of microstructural evolution in polycrystalline materials, Phys. Rev. E 76 (2007) 056702.
[181] S. Vedantam, B. Patnaik, Efficient numerical algorithm for multiphase field simulations, Phys. Rev. E 73 (2006) 016703.
[182] J. Simmons, C. Shen, Y. Wang, Phase field modeling of simultaneous nucleation and growth by explicitly incorporating nucleation events, Scr. Mater. 43 (2000) 935–942.
[183] Y. Wen, J. Simmons, C. Shen, C. Woodward, Y. Wang, Phase-field modeling of bimodal particle size distributions during continuous cooling, Acta Mater. 51 (2003) 1123–1132.
[184] J. Gibbs, Collected Works, vol. 1, Yale University Press, New Haven, Connecticut, 1948.
[185] L. Gránáy, T. Pusztai, J.A. Warren, Modelling polycrystalline solidification using phase field theory, J. Phys.: Condens. Matter 16 (2004) R1205–R1235.
[186] L. Gránásy, T. Pusztai, D. Saylor, J. Warren, Phase field theory of heterogeneous crystal nucleation, Phys. Rev. Lett. 98 (2007) 035703.
[187] H. Emmerich, R. Siquieri, Investigating heterogeneous nucleation in peritectic materials via the phase-field method, J. Phys.: Condens. Matter 18 (2006) 11121–11129.
[188] L. Gránásy, T. Pusztai, G. Tóth, Z. Jurek, M. Conti, B. Kvamme, Phase field theory of crystal nucleation in hard-sphere liquid, J. Chem. Phys. 119 (2003) 10376–10382.
[189] C. Shen, Q. Chen, Y.H. Wen, J.P. Simmons, Y. Wang, Increasing length scale of quantitative phase field modeling of growth-dominant or coarsening-dominant process, Scr. Mater. 50 (2004) 1023–1028.
[190] J. Zhu, T. Wang, S. Zhou, Z. Liu, L. Chen, Quantitative interface models for simulating microstructure evolution, Acta Mater. 52 (2004) 833–840.
[191] J. Zhu, T. Wang, A. Ardell, S. Zhou, Z. Liu, L. Chen, Three-dimensional phase-field simulations of coarsening kinetics of γ' particles in binary Ni–Al alloys, Acta Mater. 52 (2004) 2837–2845.
[192] R. Folch, M. Plapp, Quantitative phase-field modeling of two-phase growth, Phys. Rev. E 72 (2003) 011602.
[193] A. Kazaryan, Y. Wang, S.A. Dregia, B.R. Patton, Generalized phase-field model for computer simulation of grain growth in anisotropic systems, Phys. Rev. B 61 (2000) 14275–14278.
[194] J. Collins, H. Levine, Diffuse interface model of diffusion-limited crystal growth, Phys. Rev. B 31 (1985) 6119–6122.
[195] G. Caginalp, W. Xie, Phase-field and sharp-interface alloy models, Phys. Rev. E 48 (1993) 1897–1908.
[196] K. Elder, M. Grant, N. Provatas, J. Kosterlitz, Sharp interface limits of phase-field models, Phys. Rev. E 64 (2000) 021604.
[197] R. Almgren, Second-order phase field asymptotics for unequal conductivities, SIAM, J. Appl. Math. 59 (1999) 2086–2107.
[198] D. Fan, L.-Q. Chen, Diffuse-interface description of grain boundary motion, Phil. Mag. Lett. 75 (1997) 187–196.
[199] C. Shih, M. Lee, C. Lan, A simple approach toward quantitative phase field simulation for dilute-alloy solidification, J. Cryst. Growth 282 (2005) 515–524.
[200] K. Elder, M. Katakowski, M. Haataja, M. Grant, Modeling elasticity in crystal growth, Phys. Rev. Lett. 88 (2002) 245701.
[201] K. Elder, M. Grant, Modeling elastic and plastic deformation in nonequilibrium processing using phase field crystals, Phys. Rev. E 70 (2004) 051605.
[202] K. Elder, N. Provatas, J. Berry, P. Stefanovic, M. Grant, Phase-field crystal modeling and classical density functional theory of freezing, Phys. Rev. E 75 (2007) 064107.
[203] J. Berry, M. Grant, K. Elder, Diffusive atomistic dynamics of edge dislocations in two dimensions, Phys. Rev. E 73 (2006) 031609.